

5-1-2019

Comparitive Analysis in Non-linear Model of Pre-stressed Concrete Beam

Xingjian Wang
Lehigh University, wangxingjian112@gmail.com

Follow this and additional works at: <https://preserve.lehigh.edu/etd>



Part of the [Civil Engineering Commons](#)

Recommended Citation

Wang, Xingjian, "Comparitive Analysis in Non-linear Model of Pre-stressed Concrete Beam" (2019).
Theses and Dissertations. 5711.
<https://preserve.lehigh.edu/etd/5711>

This Thesis is brought to you for free and open access by Lehigh Preserve. It has been accepted for inclusion in Theses and Dissertations by an authorized administrator of Lehigh Preserve. For more information, please contact preserve@lehigh.edu.

Comparitive Analysis in Non-linear Model of Pre-stressed Concrete Beam

by

Xingjian Wang

A Thesis

Presented to the Graduate and Research Committee

of Lehigh University

in Candidacy for the degree of

Master of Science

in

MS, Structural Engineering

Lehigh University

(May, 2019)

© 2019 by Xingjian Wang

Lehigh University, Spring Semester

This thesis is accepted and approved in partial fulfillment of the requirements for the Master of Science.

Date

Thesis Advisor: Dr. Paolo Bocchini

Co-Advisor: Dr. Alfred Strauss

Chairperson of Department: Dr. Panos Diplas

ACKNOWLEDGEMENTS

I would like to thank sincerely Dr. Bocchini and Dr. Strauss, my advisor and co-advisor, for their continuous guidance. It is pleasant for me to work with them, correcting the results and discussing the next step. I also want to thank the research group covering USA and Europe, including my advisor and co-advisor, Dr. Sousa, Benjamin and Daniel (students of Dr. Strauss) and Emanuele and Wazeer (students of Dr. Sousa). This group is arranged to have a video meeting every two weeks and in this meeting we can renew our research work, discuss it and receive some good suggestions, which is quite useful to me. Finally I would like to thank my parents for their financial and mental support to me. Without their encouragement I may not finish my study successfully like this.

Contents

Abstract.....	1
Chapter 1 Introduction.....	2
Chapter 2 Experimental Testing.....	6
2.1 Material, geometry and reinforcement layout.....	6
2.2 Monitoring points.....	11
Chapter 3 Numerical Non-linear Finite Element Models.....	12
3.1 Numerical model in ATENA Engineering.....	12
3.1.1 Geometry.....	12
3.1.2 Material model.....	16
3.1.3 Loading and pre-stressing.....	20
3.1.4 Verification of accuracy for the three-dimensional (3D) finite element model	23
3.2 Numerical model in ABAQUS.....	33
3.2.1 Geometry.....	33
3.2.2 Material.....	34
3.2.3 Analysis steps and results.....	37
Chapter 4 Mesh and Mesh Alignment in ATENA Engineering.....	41
4.1 General analysis for mesh sensitivity problem.....	41
4.2 Nodal distance.....	56
Chapter 5 Differences in commercial software products.....	65
Chapter 6 Conclusion.....	69
References.....	71
Chapter 7 Brief biography.....	73

List of tables

Table 2-1 Casting and testing procedure for the determination of the stochastic properties E_c (Elastic modulus), f_{ct} (tensile strength of concrete), G_f (shear energy) and f_c (compressive strength of concrete) of the 10 laboratory beams. (β_D and β_{BZ} represent different types of specimens). Adapted from Strauss et al. (2017).	7
Table 2-2 Statistics of the parameters of the concrete of class C50/60 with age 28 days.	8
Table 2-3 Detailed list of the reinforcement present in T-shaped beam (adapted from Strauss et al. 2017).	10
Table 3-1 Total loading procedure.	22
Table 3-2 The model updating process for FE analysis in ATENA Engineering.	24
Table 3-3 Concrete parameters in ABAQUS.	36
Table 3-4 Steel parameters in ABAQUS (reinforcement not included).	36
Table 3-5 Reinforcement parameters in ABAQUS.	37
Table 3-6 Pre-stressing tendon parameters in ABAQUS.	37
Table 3-7 Loading procedure in ABAQUS.	39
Table 4-1 Mesh and material parameters in Case 1.	45
Table 4-2 Interpolation function for the contact between nodes.	47
Table 4-3 Displacement of different mesh patterns at point 16.	51
Table 4-4 Displacement of different mesh patterns at point 15.	51
Table 4-5 Comparison of 3 test cases.	54

List of figures

Figure 2-1 Mean value of reinforcement (BST550) and pre-stressing tendons (ST1570/1770) (adapted from Strauss et al. 2017).	8
Figure 2-2 The geometry of the beam (adapted from Strauss et al. 2017).	9
Figure 2-3 Comparison of idealized and real cross-section (left part is the real section and right part is the idealized section). Adapted from Strauss et al. (2017).	9
Figure 2-4 The detailed reinforcement (adapted from Strauss et al. 2017).	10
Figure 2-5 The monitoring points used in the test (adapted from Strauss et al. 2018).	11
Figure 3-1 The reinforcement layout and generated mesh in ATENA.	14
Figure 3-2 Different models for the connection.	15
Figure 3-3 Difference in dealing with the slab by considering it (a) as a whole region discretized with shell elements and (b) as an assemblage of parts, with bricks at the center and shells at the sides.	15
Figure 3-4 Material parameters of reinforcement.	17
Figure 3-5 Material parameters of tendons.	17
Figure 3-6 Material parameters of the concrete.	19
Figure 3-7 Material parameters of steel plates.	19
Figure 3-8 Load-Displacement relationship of the model.	23
Figure 3-9 Objective function in the form of the minimized difference of load-displacement curve in area between the experimental measurement and the numerical model.	24
Figure 3-10 The result for V1 model.	25
Figure 3-11 The result for V2 model.	26
Figure 3-12 The result for V3 model.	27
Figure 3-13 Comparison of mesh pattern for model V3 and V4.	28
Figure 3-14 The result for V4 model.	29
Figure 3-15 The force-strain relationship of the model.	31

Figure 3-16 Load-Displacement relationship of V5 model.	32
Figure 3-17 Detailed mesh generation of the model.	34
Figure 3-18 Final version of numerical model in ABAQUS.	40
Figure 4-1 Poor mesh in the model by using automatic generation.	43
Figure 4-2 Geometry and two different mesh patterns for the mesh case study 1.	44
Figure 4-3 Local coordinates of each element.	46
Figure 4-4 Local coordinates when dealing with the contact between macro elements.	46
Figure 4-5 Poor mesh with all nodes numbered.	47
Figure 4-6 Stress distributions calculated by using algorithm above.	49
Figure 4-7 Stress distributions for Case 1 in ABAQUS with finer mesh.	50
Figure 4-8 Difference between good mesh and poor mesh.	51
Figure 4-9 The stresses along the contact.	52
Figure 4-10 The displacements along the contact.	53
Figure 4-11 General appearance of 2 dimensional poor mesh.	53
Figure 4-12 Detailed information about Case 4.	54
Figure 4-13 Stress and displacement developments along the contact with nodal distance increasing in ABAQUS.	59
Figure 4-14 The stress and displacement developments along the contact with nodal distance increasing in ATENA Engineering.	62
Figure 4-15 Development of stress and displacement at middle point along with nodal displacement Δ increasing.	63
Figure 5-1 Comparison of stress distributions with and without contact.	66
Figure 5-2 Comparison of stress with and without the contact.	66

List of symbols

E_c	Elastic modulus of concrete (MPa)
f_{ct}	Tensile strength of concrete (MPa)
G_f	Shear energy of concrete (MN/m)
f_c	Compressive strength of concrete (MPa)
β_D & β_{BZ}	Two different types of specimens

Abstract

The author presents a detailed procedure to model a pre-stressed concrete beam in ATENA Engineering and ABAQUS, considering a series of load cases. One of the main purposes of the thesis is to investigate the time effort required and the additional knowledge gained by modeling techniques of increasing accuracy, and based on different software packages. The two software packages differ in several substantial ways: mechanical models available, visualization, time costs, primary fields of application, and models for concrete cracking. This effort is part of a larger initiative with contributors from the USA and Europe to study the value of advanced modeling within the life-cycle cost of a major structure. Moreover, the thesis focuses on numerical problems arising from independent meshing of the multiple parts of the beam. Sensitivity analyses are performed to evaluate the effect of misalignment of the various local meshes on the global failure modes of the beam.

Keywords: beam models, experimental results, sensitivity analysis, finite element software and models.

Chapter 1 Introduction

Reinforced concrete is a basic construction material used everywhere in the world, but its complex properties still require a lot of researches, its crack propagation, its shrinkage and creep, its non-linear mechanical behavior. In the past 50 years many analyses about the behaviors of reinforced concrete were published (Tong et al. 2016 [1]).

My co-advisor, Dr. Alfred Strauss has worked on a comprehensive model updating procedure for pre-stressed concrete beams, including their combined shear and flexure capacity. He developed a monitoring and modeling system that can capture the crack behavior both in experiments and numerical models. An example application of this approach was presented in [2], where Dr. Strauss and his collaborators modeled a pre-stressed concrete beam. In such paper, the assessment of accuracy was done focusing on three parameters: the load displacement curve, the crack pattern, and strains measured by electric strain gages (ESG). The process is presented through 7 model refinements, each improving on the previous. In [2], the numerical non-linear finite element model is presented step-by-step, including aspects related with the support conditions, accurate cross-section, optimized mesh, adjusted material parameters, losses due to changes in elastic modulus and losses due to rheological features, such as shrinkage and creep of concrete over time. Emphasis is put on how to model a pre-stressed concrete beam more accurately, and all of these efforts are based on the ATENA Science and GID [3] software packages. One of the goals of this thesis is to investigate

how these models need to be adjusted when other software packages are used, such as ABAQUS, ANSYS and so on. Besides, in his paper an unsymmetrical load was added on the beam and Dr. Strauss cut the beam into two parts with condensed mesh in the loading part (to obtain a precise shear break), but doesn't prove its rationality that this change will do much effect on the final result (2017).

One of the critical steps to capture correctly the mechanical behavior appeared to be the finite element mesh. Many researchers have worked in the field of mesh sensitivity, not only working on the size of the elements, but the location of the nodes. For instance, Needleman [4] analyzed the localization problems with material rate independency and mesh sensitivity in a simple one-dimension problem. The incremental equilibrium equations for quasi-static problems remain elliptic and wave speeds for dynamic problems stay real in the circumstance of strain rate independent solid. At this time, the pathological mesh sensitivity associated with numerical solutions of localization problems can be eliminated. But in his paper he elaborated at length on material rate independency, with few words on mesh sensitivity problems, and he didn't mention clearly how the pathological mesh sensitivity look like and how we can do to deal with it. Munjiza [5] gives us a general method to calculate the sensitivity of mesh size in a combined single and smeared fracture problem. In his examples a square plate with bilinear material is meshed in triangular shell elements, it has a crack open with $1/3$ edge length in the middle of geometry, suffering tensile loads on the opposite two edges. He reduced the mesh size to obtain an optimal size which had an accurate result with the least number of elements. From the theoretical solutions we can obtain a valid and

satisfied element size that can provide a good result. Then he uses numerical models to confirm that the model with this mesh size can present an accurate enough result and even beyond this size the result will not get a big change when studying the failure problem. His aim is explore an optimized mesh size between accuracy and calculating time. If a large-scale engineering problem is studied with elements of size millimeters, the computational time may be impractical. But in his paper he focuses on a small-scale symmetric plate suffering symmetric tensile load at its opposite edges. It is a very simple and small example and the paper does not say anything about how large-scale complex problems can be dealt with. In addition, the method is limited in scope to 2D triangular elements, and it is not clear how it can be generalized to other 2D elements or 3D brick elements.

Some of these papers use very simple numerical models to demonstrate their analytical parts, some of them use complex models but do not provide details. In particular, for complex 3D solid models, they do not analyze the problem of multiple compounded parts, mesh compatibility, and contact models between the various parts. They do not discuss what happens if the meshes are built independently, and how this can affect the accuracy of the results. These aspects are discussed in the present thesis.

This thesis aims to provide a step-by-step procedure to build a non-linear finite element model for a prestressed beam, both in ATENA Engineering and ABAQUS, compare these results with the experimental data, and investigate two big problems in modeling a concrete beam, one is mesh sensitivity and node positions, and the other is the calculation of contact.

A step-by-step modeling guide is often neglected in scientific papers, but it constitutes an important set of information to reproduce the presented results. Papers often present only input parameters and result analysis, with no guidance on how the model is built, to assist readers in using the same example for further studies. Some example of particularly delicate modeling aspects that are discussed in the present thesis are the following.

1. The traditional non-linear FE calculation does not consider the time variance of some material parameters, like modulus of elasticity. In this thesis we get the parameters of concrete at 14 hours and 28 days separately and compare the numerical result with the experimental data in order to identify accurate parameters.
2. The cracked region of concrete is characterized by lower strength than intact concrete. However, this aspect is often ignored in traditional non-linear FE analysis. In the models presented in this thesis, the post-cracking concrete properties are changed, which results in increased accuracy.

Non-linearity in mechanical problems includes the non-linear material behavior and non-linear geometrical effects. In this research we disregard geometrically non-linear effects and we only consider material non-linearity. To address material non-linearity we use the Newton-Raphson method, which is an iterative way to account for non-linear material laws.

Chapter 2 Experimental Testing

2.1 Material, geometry and reinforcement layout

The experiment used as basis for the models presented in this thesis was performed in Austria in 2013 in the University of Natural Resources and Life Sciences and the associated Partner Laboratories. The author was informed about this experiment by his co-advisor and then decides to analyze the shear and flexure performance of concrete and the mesh sensitivity based on its data.

This experiment is a verification test. It contains two parts, the full scale girder test and the small scale beam test. The experiment aimed to analyze the shear fracture pattern and some other performances of one real girder (33m pre-stressed concrete roof element). As the full scale girder was too large and only several tests can be done due to the space and money, the small scale beam was considered to get these performance and see the clear crack development (Strauss et al. 2017).

475 concrete specimens were tested in the experiment. They were divided into two groups, one is the component storage and the other is the standard storage. For each group three cases were considered, C50/60, C40/50 (reference [6]) and the specimens cast along with laboratory beams (5 meters T-shaped beam) C50/60, where C50/60 and C40/50 are the types of concrete in Europe. For each case the detailed information is provided in Tables 2-1 and 2-2 below.

Table 2-1 Casting and testing procedure for the determination of the stochastic properties E_c (Elastic modulus), f_{ct} (tensile strength of concrete), G_f (shear energy) and f_c (compressive strength of concrete) of the 10 laboratory beams. (β_D and β_{BZ} represent different types of specimens). Adapted from Strauss et al. (2017).

Fracture test – component storage
C50/60
<p><u>70 specimens:</u> $21 \cdot \beta_{D150 \times 150 \times 150}(f_c)$; $28 \cdot \beta_{BZ100 \times 100 \times 400}(f_c, E_c, G_f)$; $21 \cdot G_{F150 \times 150 \times 150}(G_f)$</p> <p><u>Tested:</u> 1d (β_{BZ}, G_F); 7d (β_D, β_{BZ}); 28d (β_D, β_{BZ}, G_F); 126d (β_D, β_{BZ}, G_F)</p>
C40/50
Similar to C50/60
Specimens casted along with laboratory beams C50/60
<p>120 specimens: $6 \cdot \beta_{D150 \times 150 \times 150}(f_c)$; $3 \cdot \beta_{EM100 \times 100 \times 360}(E_c)$; $3 \cdot \beta_{SZ120 \times 120 \times 360}(f_{ct,sp})$</p> <p>Tested: 28d ($\beta_D$); 33d ($\beta_D, \beta_{EM}, \beta_{SZ}$)</p>
Fracture test – standard storage
C50/60
<p>14 specimens: $7 \cdot \beta_{BZ100 \times 100 \times 400}(f_c, E_c, G_f)$; $7 \cdot G_{F150 \times 150 \times 150}(G_f)$</p> <p>Tested: 28d ($\beta_{BZ}, G_F$)</p>
C40/50
Similar to C50/60
Specimens casted along with laboratory beams C50/60
<p>19 specimens: $10 \cdot \beta_{D150 \times 150 \times 150}(f_c)$; $5 \cdot G_{F150 \times 150 \times 150}(G_f)$; $4 \cdot \beta_{BZ120 \times 120 \times 360}(f_c, E_c, G_f)$</p> <p>Tested: 7d ($\beta_D$); 21d ($\beta_D, G_f, \beta_{BZ}$)</p>

Table 2-2 Statistics of the parameters of the concrete of class C50/60 with age 28 days.

Parameter	Mean	COV (%)	PDF
Compressive strength	77 MPa	6.4	GMB min EV 1
Tensile strength	3.9 MPa	10.6	GMB max EV 1
Modulus of elasticity	34.8 GPa	10.6	WBL min (3 par)
Fracture energy	219.8 J/m ²	12.8	GMB max EV 1

Due to the randomness in their properties, more than 100 tests were done for the material used for steel bars and tendons. The reinforcement consists of mildsteel bars BST550 and the pre-stressing steel consists of strands ST1570/1770 (two material types of reinforcement and tendons). Picking the mean values of these materials, their stress-strain relationships are presented in Figure 2-1.

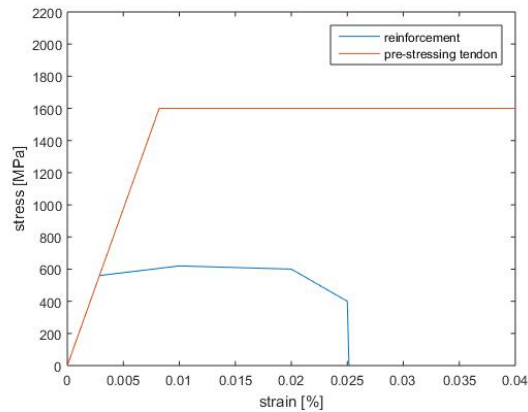


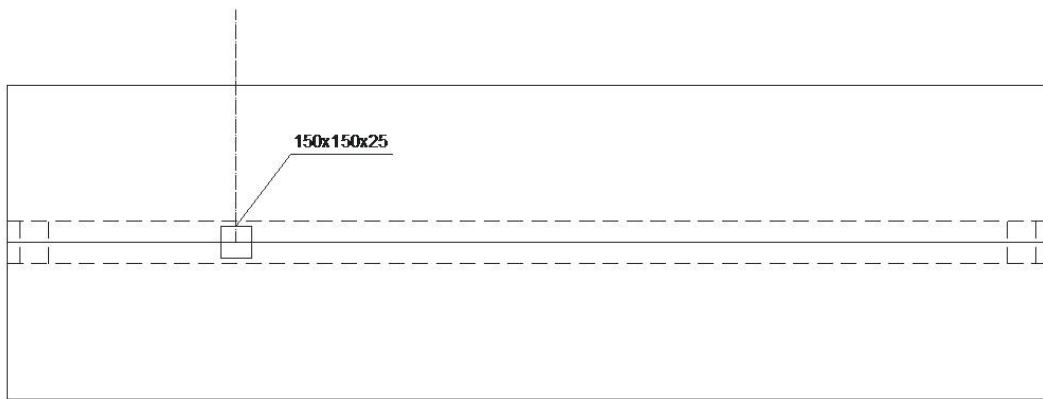
Figure 2-1 Mean value of reinforcement (BST550) and pre-stressing tendons (ST1570/1770) (adapted from Strauss et al. 2017).

The geometry of the beam is shown in Figures 2-2 and 2-3. In particular, Figure 2-3 shows that the cross section had a smooth, rounded connection between deck and web, but it was idealized using a polygonal transition when modeling. More details on the

modeling aspects will be covered in Chapter 3.



(a) the sketch of beam at side view.



(b) the sketch of beam at top view.

Figure 2-2 The geometry of the beam (adapted from Strauss et al. 2017).

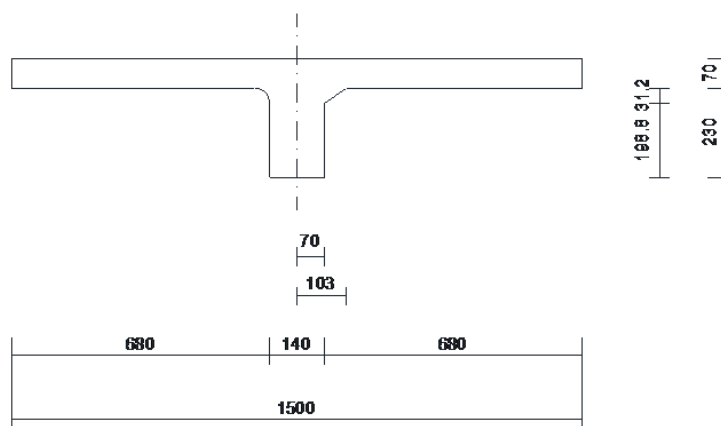


Figure 2-3 Comparison of idealized and real cross-section (left part is the real section and right part is the idealized section). Adapted from Strauss et al. (2017).

For the reinforcement, 71 steel bars and tendons were used in one small scale beam. The detailed reinforcement layout and the list of the reinforcement present in the beam are shown in Figure 2-4.

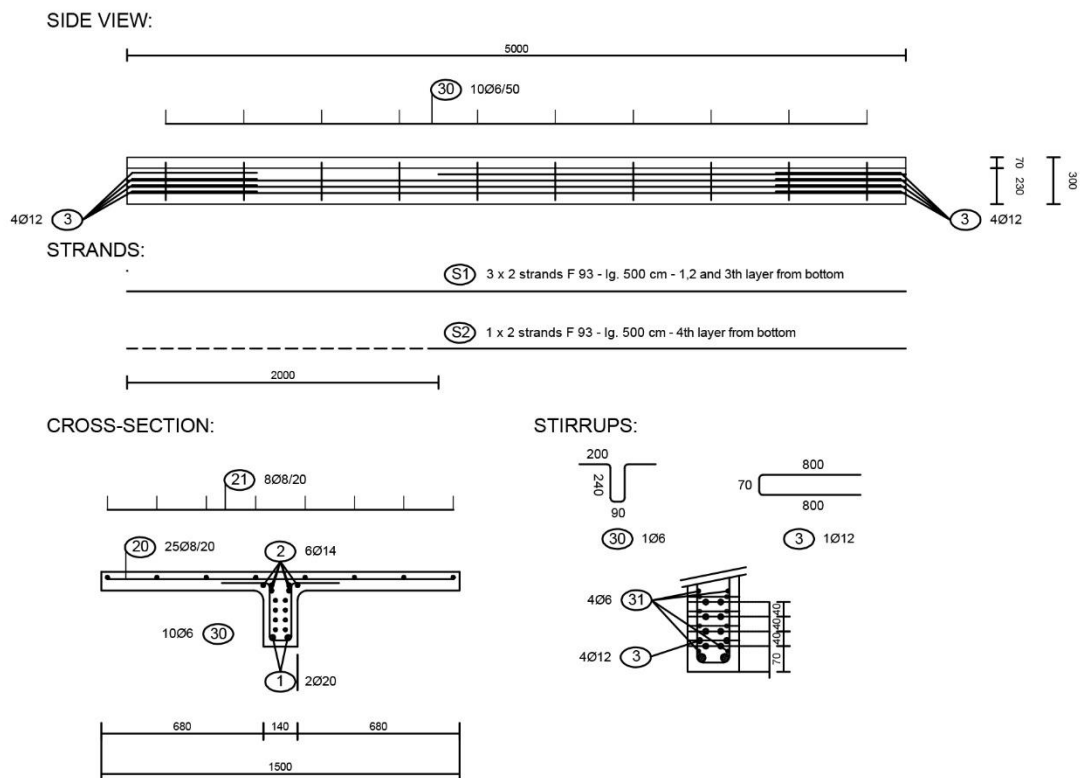


Figure 2-4 The detailed reinforcement (adapted from Strauss et al. 2017).

Table 2-3 Detailed list of the reinforcement present in T-shaped beam (adapted from Strauss et al. 2017).

Position of bars	Number of bars	Type	Φ [mm]	Individual length [m]	Mass [kg]
1	2	Rebars	20	4.95	24.45
2	6	Rebars	14	4.95	35.94
3	8	Rebars	12	1.67	11.86
30	10	Stirrups	6	0.97	2.15
31	4	Rebars	6	4.95	4.40

20	25	Rebars	8	1.45	14.32
21	8	Rebars	8	4.95	15.64
S1	6	Strands	12.5	5.00	21.78
S2	2	Strands	12.5	3.00	4.36

2.2 Monitoring points

The monitoring system shown in Figure 2-5 was prepared for each laboratory-tested beam. 13 electrical strain gages (ESG) were attached to longitudinally and vertically oriented reinforcement bars located in the shear field. A digital image correlation (DIC) system was used in this experiment. The DIC system has a great potential for efficiently monitoring structural behavior. More details on its advantages are provided in the paper by Strauss et al. 2018 (reference [7]).

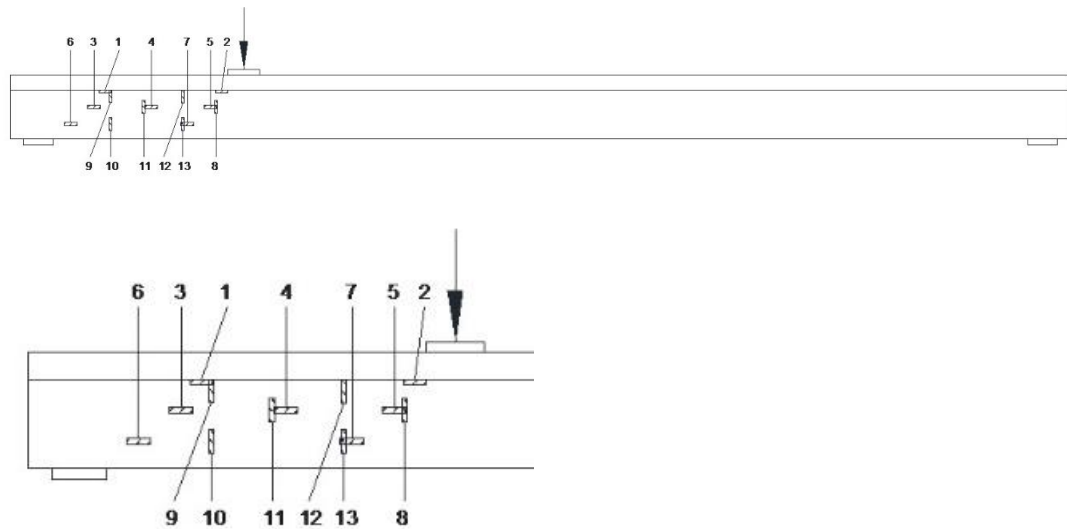


Figure 2-5 The monitoring points used in the test (adapted from Strauss et al. 2018).

Chapter 3 Numerical Non-linear Finite Element Models

The experimental results give us insight on the load transfer process and the true crack pattern. Besides this, the test of the T-shape reinforced concrete beam can also provide validation for the concrete failure mode.

The non-linear FE modeling is a very useful tool in assessing the behavior of structures and investigate potential many prestressing problems. This is much faster than the real experiment in the laboratory. But users often simplify their numerical models of real structures, sometimes using inaccurate parameters, sometimes oversimplifying the geometry, sometimes applying a wrong load pattern or loading process. These issues exist in all numerical simulations and their influence is not always clarified, especially when one approximation compounds with another. It may become a serious problem, lead to wrong result and cause substantial losses if the analyst relies exclusively on the numerical model. The idea of this Chapter is to discuss some significant aspects of numerical modeling that will cause important changes in the final results.

3.1 Numerical model in ATENA Engineering

The following sections describe how a model of the described beam can be built in the ATENA Engineering software package.

3.1.1 Geometry

The geometry of the reinforced concrete beam is provided by the manufacturer or the

designer. The shape of the cross-section is simplified using a polygonal transition between flange and web. The prismatic body extends longitudinally and the ratio of the transition angle from slab to web is no higher than 3:1. The basis for this simplification (changing the arc connection to a polygonal transition) is the fact that the cross-sectional area is preserved.

Solid elements are used in this model, with linear geometrical properties. For the finite element mesh, about 22,000 hexahedral elements are generated in ATENA Engineering. A fine mesh will increase the accuracy of the final result and reduce the calculating time, compared with the whole model in larger element size or smaller element size. Here I separate the whole beam into two parts, at $\frac{3}{5}$ of its length, one with the loading plate (left part) and the other without (right part). The pre-stressed concrete is expected to fail in shear, and the main shear zone occurs in left part. So I refined the mesh at this area, with element size of approximately 25mm. The element size of the other part, where stress patterns are easier to capture is 35mm. The ratio of the edge lengths of the smaller element is no larger than 3:1. Using this method the model will be generated less elements than the whole beam with 30 mm mesh size, and this saves a lot of time in calculation. We also tested a coarser mesh: while the resulting load-displacement curve captures well the experimental results, its cracking pattern is not as well represented as with the fine mesh. So we choose to proceed with the finer mesh size. The element type for the concrete is prismatic eight-node brick element, while for these steel plates we used tetrahedral elements. As the steel plates are thinner than the concrete, the calculation cannot work very well if we set both of them as brick elements,

and the nodes in the steel plates are hard to connect to those in the concrete surface. For the reinforcement, the software can generate an appropriate mesh, surrounded by the concrete mesh, automatically, and its boundary condition is set by default as perfect bound (embedded into the concrete). The generated mesh is shown in Figure 3-1.

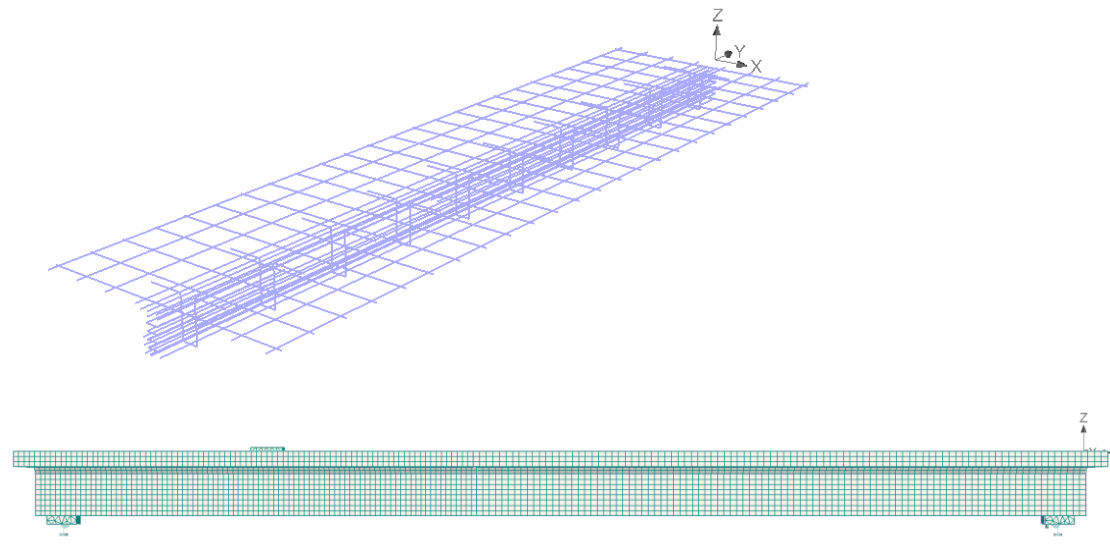


Figure 3-1 The reinforcement layout and generated mesh in ATENA.

There are two significant aspects in this model, the first is the transition region between the slab and web. In the real beam used for the experiment, there was a rounded connection (arc) from the slab to the web, but in ATENA Engineering we cannot do the same modeling because it is impossible to have an arc transition in this software. Here we have two modeling options: (a) using one layer of connecting elements with quadrilateral section (Figure 3-2a) and (b) using several thin layers of elements with different width to simulate the arc (Figure 3-2b). Based on the experimental results and analytical considerations, we decided to use the simple transition model with a small amount of polylines line in Figure 3-2a, also due to the contact problems discussed in

Chapter 4. Moreover, for option (b), if too many layers of elements are used, each layer would be better represented by a shell element, and the crack development along its thickness would not be accurate. For all these reasons, option (a) was chosen.

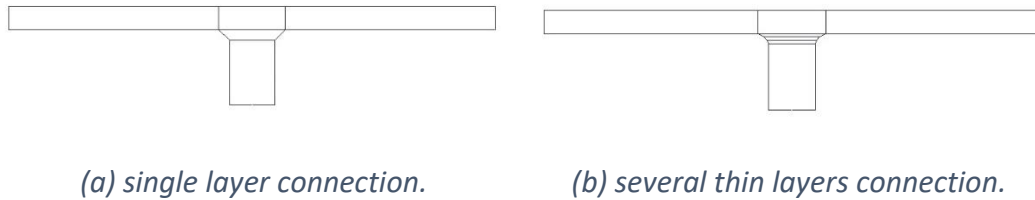


Figure 3-2 Different models for the connection.

The second important issue to consider is the discretization of the slab. As the ratio of the dimensions of the slab is 5:1.5:0.07, the whole slab can be considered as a shell. to connect shell elements with brick elements in the web, the best option is to divide the slab into three portions, adding a central region with brick elements connected to the transition part (towards the web) and to the shell elements on the sides (see Figure 3-3). This method aims to connect brick and shell elements only on their sides (from partial contact to full contact) which can reduce the calculation error.

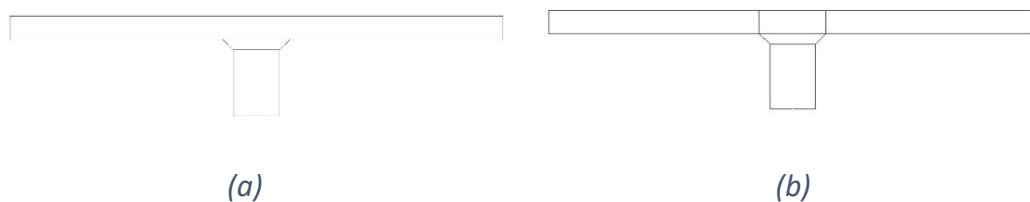
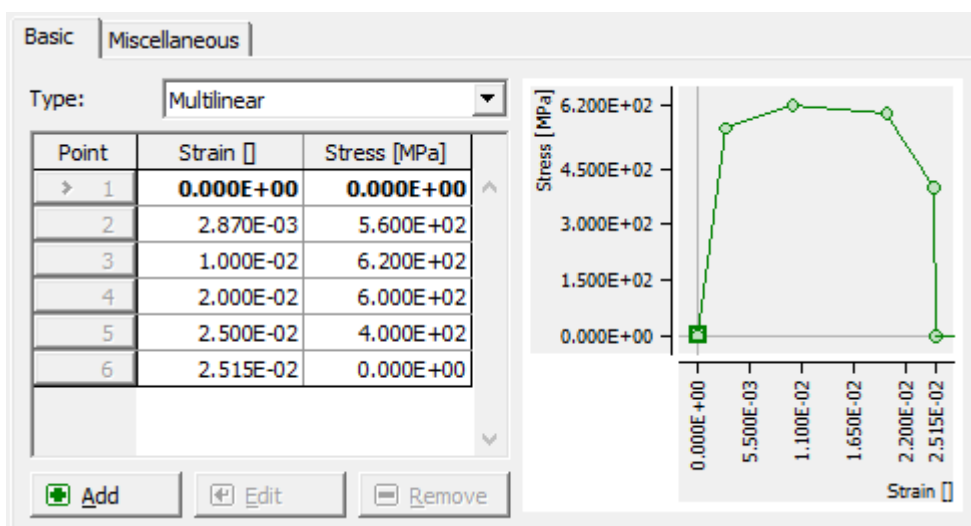


Figure 3-3 Difference in dealing with the slab by considering it (a) as a whole region discretized with shell elements and (b) as an assemblage of parts, with bricks at the center and shells at the sides.

The loading force is added in the middle of a loading plate of size 150 x 150 x 25 mm (shown in Figure 2-2). The connections between concrete and steel plates are master-slave rigid contacts.

3.1.2 Material model

The reinforcement steel bars and tendons are modeled with 1D element, their stress-strain relationship is shown in Figure 3-4. The stirrups and steel bars are modeled with the Multilinear Reinforcement material with modulus of elasticity (the first slope) equal to 195 GPa. For tendons, the Bilinear Reinforcement material is used with elastic modulus $E = 195$ GPa and yielding stress 1600 MPa. The density of reinforcement and tendons is 7850 kg/m^3 and the coefficient of thermal expansion is $1.2 \times 10^{-5} \text{ C}^{-1}$. The detailed layout is shown in Figures 3-4 and 3-5.



Basic	Miscellaneous
Specific material weight ρ :	7.850E-02 [MN/m ³]
Coefficient of thermal expansion α :	1.200E-05 [1/K]

Figure 3-4 Material parameters of reinforcement.

Basic	Miscellaneous
Type:	Bilinear
Elastic modulus E :	1.950E+05 [MPa]
σ_y :	1600.000 [MPa]

Basic	Miscellaneous
Specific material weight ρ :	7.850E-02 [MN/m ³]
Coefficient of thermal expansion α :	1.200E-05 [1/K]

Figure 3-5 Material parameters of tendons.

The material model 3D Nonlinear Cementitious 2 is used for the concrete. The most important parameters are its compressive strength, tensile strength, modulus of elasticity, and fracture energy. From the measurements in experimental tests, accurate values of these parameters are obtained. These significant parameters are shown in the panels of Figure 3-6.

Edit material "3D Nonlinear Cementitious 2" n.3

Material name
Title: Concrete

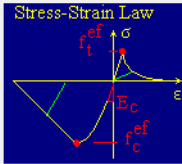
Basic | Tensile | Compressive | Shear | Miscellaneous

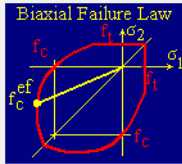
Elastic modulus E: 2.843E+04 [MPa]

Poisson's ratio μ : 0.200 [-]

Tensile strength f_t : 3.343E+00 [MPa]

Compressive strength f_c : -6.970E+01 [MPa]

Stress-Strain Law 

Biaxial Failure Law 

Number: 3

OK Cancel

Edit material "3D Nonlinear Cementitious 2" n.3

Material name
Title: Concrete

Basic | Tensile | Compressive | Shear | Miscellaneous

Specific fracture energy G_F : 1.970E-04 [MJ/m]

Crack spacing s_{max} : [m]

Tension stiffening c_{sp} : [-]

Unloading: [-]

Number: 3

OK Cancel

Edit material "3D Nonlinear Cementitious 2" n.3

Material name
Title: Concrete

Basic | Tensile | Compressive | Shear | Miscellaneous

Critical compressive displacement W_d : -5.000E-04 [m]

Plastic strain at compressive strength ϵ_{cp} : -2.894E-03 [-]

Reduction of comp. strength due to cracks $r_{c,lim}$: 0.8 [-]

Number: 3

OK Cancel

Edit material "3D Nonlinear Cementitious 2" n.3

Material name
Title: Concrete

Basic | Tensile | Compressive | Shear | Miscellaneous

Crack Shear Stiff. Factor S_F : 100.0 [-]

Aggregate Interlock MCF

Aggregate size: 0.020 [m]

Number: 3

OK Cancel

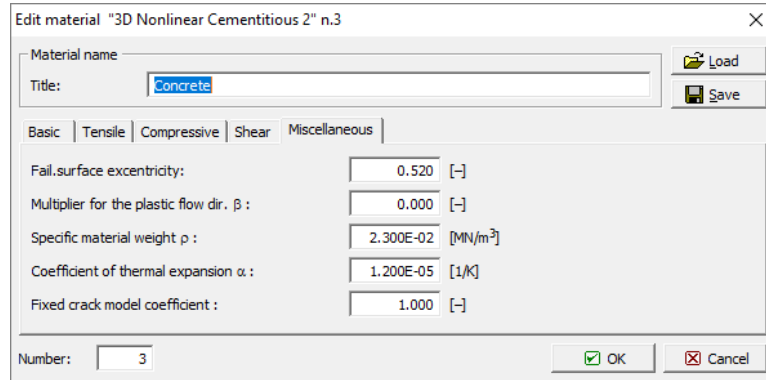


Figure 3-6 Material parameters of the concrete.

For the steel plates (one loading plate and two support plates), since the stress inside is much lower than its elastic limit, the 3D Elastic Isotropic material is used in ATENA Engineering with elastic modulus of 28.483 GPa, which unrealistic for steel, but is the same used for concrete, in order to get a simultaneous deformation between steel plates and the main concrete beam. All the parameters are shown in Figure 3-7, with Poisson's ratio, material weight and the coefficient of thermal expansion.

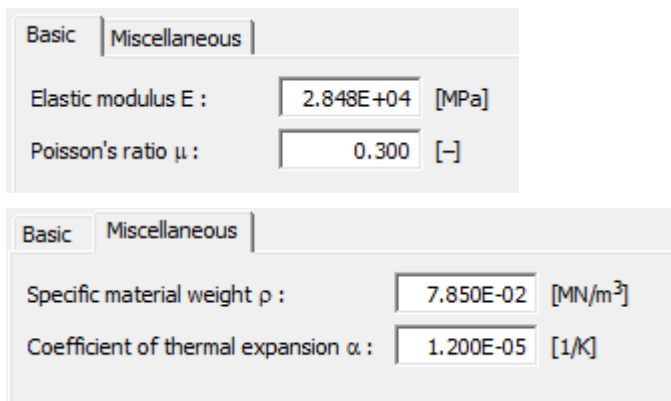


Figure 3-7 Material parameters of steel plates.

3.1.3 Loading and pre-stressing

The loading procedure includes four items: the internal load (self-weight), the pre-stressing load, the temperature and the vertical load. For these four load types, detailed information is provided in the following.

The first loading is the internal load (self-weight). I applied the concrete specific weight as 2300kg/m^3 . The “monitors” used by ATENA to record strains are put in place along the reinforcement bars before the application of the self-weight. These monitors are set to obtain the strain increments in the steel bars, in order to compare them with the experimental results collected at the same locations. This allows us to check the accuracy of the model. In practice, the experimental monitor is a 4-mm-long electric strain gage, while in the numerical model it is just a monitoring point. In the case of crack development occurring precisely where a 4-mm-long strain gage is placed, the measurement will result in the increase of the strain in the steel bar. However, as the monitoring point in the numerical model is an actual point, it is more difficult for it to capture the development of cracks. There are strategies to detect the presence of the crack, looking at the change in slope of the strain time history. The most relevant piece of information is the time at which the stiffness changes, and this should be well captured by the model, it should match what was measured during the experiment. Going back to the loading process, since in ATENA Engineering each loading step is added to the structure instantaneously (not a ramped increase), the self-weight is divided into 10 steps, in order to obtain a smooth loading procedure (the same reasoning applies to the following loading processes).

The second loading is the pre-stressing load. There are two different methods to add pre-stress, one is adding it before the vertical load and the other is adding it together with the vertical load. The two methods have some only a small difference. The first one, pre-stressing before loading, may cause some additional small cracks that would never happen in reality. This is the reason why in reality we cast the concrete after pre-tensioning the tendons, but in the numerical model we can just construct the whole model and then add the pre-stress. The real procedure cannot be represented in the model because of its inherent sequence and this may cause some cracks that are realistic, and may mislead the interpretation of the results. The second method, pre-stressing together with the vertical load, is not a realistic procedure. In particular, this can be done, for instance, dividing the whole pre-stressing load into 10 steps, and adding a small vertical load increment between two pre-stressing steps. Although it is different from reality, it is better in controlling the formation of small cracks mentioned before. After comparing these two methods, I concluded that this small change does not affect significantly the final result, which means that the small cracks can be neglected when using the first method. So I choose the first method in the final model, to better represent the real processes followed in the experiment.

The third loading is the temperature. For this part we need to consider the shrinkage and creep of concrete. We have to consider not only the temperature change, but also the simultaneous pre-stressing loss. From the experimental test, we learn that twenty percent of the pre-stress is lost in 41 days of hardening. This may be caused by the decrease in temperature, the shrinkage or creep, or just the long-term pre-stressing loss.

We do not know the exact cause of this pre-stress loss (it is likely a combination of multiple causes), but the reason is irrelevant. The important aspect is the amount of pre-stress loss, which can be input into the numerical model to improve the accuracy of the calculations.

The fourth loading item is the vertical load, which in this case is the main load that we consider. For this part we have two different approaches to the incremental analysis: (a) loading using force-control and (b) loading using prescribed displacement (displacement control). Both approaches can provide similar results, but we cannot increment the load beyond its ultimate value. For this reason only the displacement-controlled loading can capture the post-peak behavior. For this certain model we do not need to consider the post-peak part, but in ATENA Engineering if we use force-control, the load-displacement curve present many small fluctuations associated with the small load increments added instantly on the model. To obtain a smoother curve, I used prescribed displacements to represent the vertical load (displacement-control). An increment of 0.1 mm per load step is chosen for this model. This small value will allow us to capture small changes. After 100 steps the load increment w is reduced to 0.05mm because this part of process includes the crack development and reducing the increment will yield a more accurate load-displacement curve. The total loading procedure is displayed in Table 3-1, and the final numerical results compared with the experimental data are shown in Figure 3-8.

Table 3-1 Total loading procedure.

Load cases	Multiplier	Step number	Steps
------------	------------	-------------	-------

Self-weight 1	0.1	1	1
Pre-stress 1	0.1	2	1
...	...	3 - 18	...
Self-weight 10	0.1	19	1
Pre-stress 10	0.1	20	1
Prescribed displacement	1	21 - 120	100
Smaller increment	1	121 - 165	45

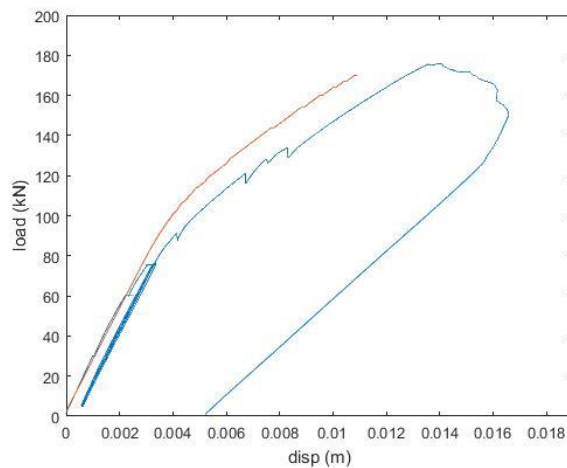


Figure 3-8 Load-Displacement relationship of the model.

3.1.4 Verification of accuracy for the three-dimensional (3D) finite element model

The methodology to verify the accuracy is based on the load-displacement diagram obtained at the selected loading point (see Figure 3-8). The main idea is to minimize the value of the discrepancy over the monitoring range from the initial to the ultimate loading capacity, for example, for this particular test T from 0 to 175 kN:

$$\min \int_0^{175} |g(F) - f(F)| dF \quad (3-1)$$

Where F represents the applied load, $g(F)$ is the load-displacement curve measured in the experimental breaking test, and $f(F)$ is the same curve obtained from the numerical simulation. Figure 3-9 presents the difference in area between experimental

measurement and numerical calculation, which is the objective function to be minimized.

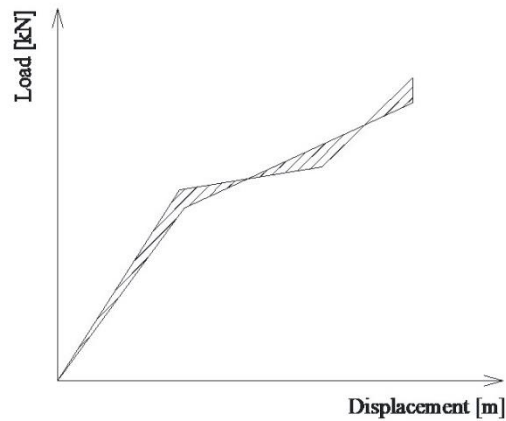


Figure 3-9 Objective function in the form of the minimized difference of load-displacement curve in area between the experimental measurement and the numerical model.

Next, we will compare and discuss different versions of the model. This comparison aims to provide argument to support these improvements and shows how much these changes influence the final result. I have built five different models and each improvement is labeled below in Table 3-2.

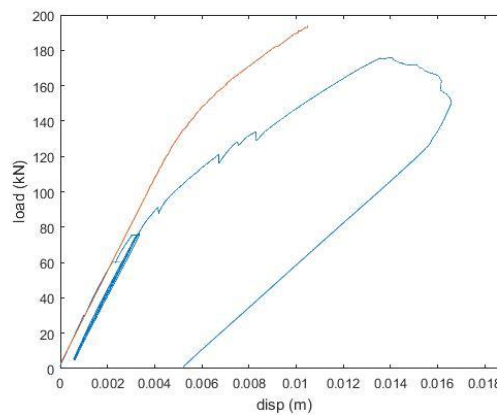
Table 3-2 The model updating process for FE analysis in ATENA Engineering.

	ATENA Engineering finite element model versions				
Improvement of models	V1	V2	V3	V4	V5
Changed cross-section	No	Yes	Yes	Yes	Yes
Pre-stressing loss	No	No	Yes	Yes	Yes
Optimized mesh	No	No	No	Yes	Yes
Modified parameters with the reason of software itself	No	No	No	No	Yes

The **first model**, 3D non-linear finite element model V1 is with linear supports. This is the basic model without any improvement in order to be used as baseline. For this model we use the initial tested parameters, a polyline with several thin prismatic bodies in the connection region, and a coarse mesh with all element size of 50mm. This is the standard and the following models are all improved versions of this. Its results for the load-displacement diagram compared with experiment data is shown in Figure 3-10.



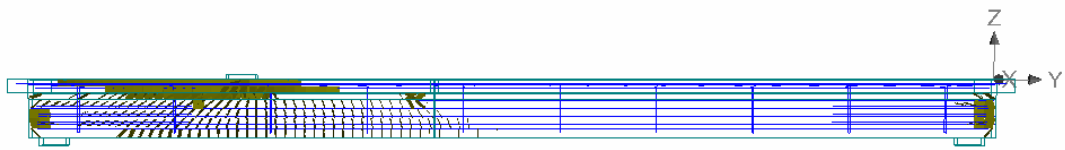
(a) breaking pattern in V1 model.



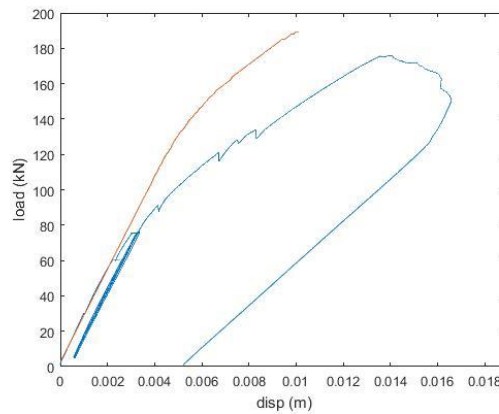
(b) Load-Displacement relationship of V1 model.

Figure 3-10 The result for V1 model.

The change in the second 3D non-linear FE **model V2** consists in an updated cross-section. In V1 I used a linear transition for the connection, but in V2, as discussed in Chapter 2, I used a simplified transition. The adjusted crack pattern development and the load-displacement diagram are shown in Figure 3-11. The difference between V1 and V2 is not very apparent, but the ultimate load is decreased from 192 kN to 185 kN.



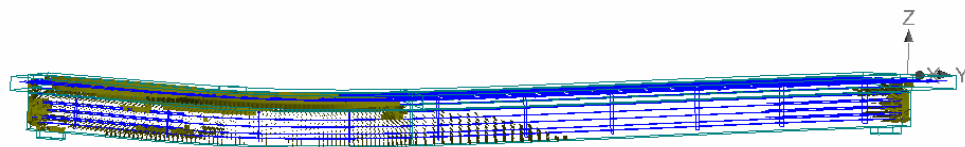
(a) *breaking pattern in V2 model.*



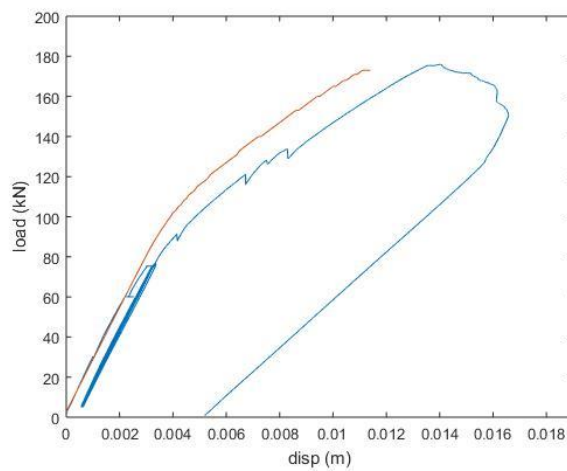
(b) *Load-Displacement relationship of V2 model.*

Figure 3-11 The result for V2 model.

The next improvement for the **third model V3** is the pre-stressing loss. This results from many factors: the temperature change, the decrease of elastic modulus E , the shrinkage and creep of concrete, and the pre-stressing loss in the long term. From the experiment, we know that the pre-stress decreases up to 20 – 40% (60 – 80% remain). Based on this test, we change the pre-stress to 641 MPa (about 20% reduction) and the improved figure of load-displacement curve is presented in Figure 3-12.



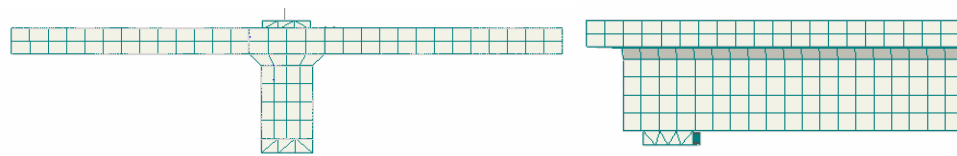
(a) breaking pattern in V3 model.



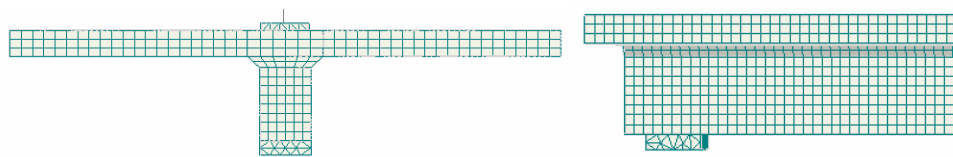
(b) Load-Displacement relationship of V3 model.

Figure 3-12 The result for V3 model.

For the **forth model V4** the main difference is the optimized, much finer mesh. In the versions V3 I only used a coarse mesh with size of 50mm. In this case I reduced its size and even changed the ratio of edges (shape control). Figure 3-13 displays the two mesh cases. The right one is a solid element with square surface in the side view and the left one changes its ratio of edges to 1:1.3 at the same viewing (with the refined mesh). Besides this, I also check the node positions along the model to confirm that the nodes are linked perfectly between macro-elements (more on this in Chapter 5). The final load-displacement curves are shown in Figures 3-14 and 3-15, and the force-strain relationship in each monitoring point is shown next (in the following figures the blue curve is the experimental data while the red one is the simulation result).

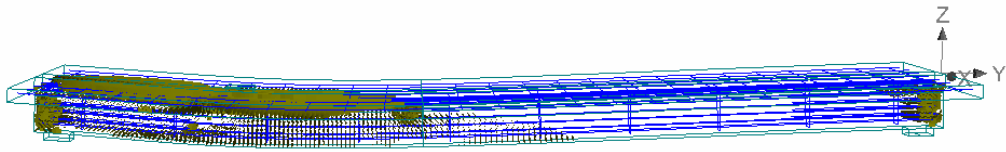


(a) mesh pattern for model V3.

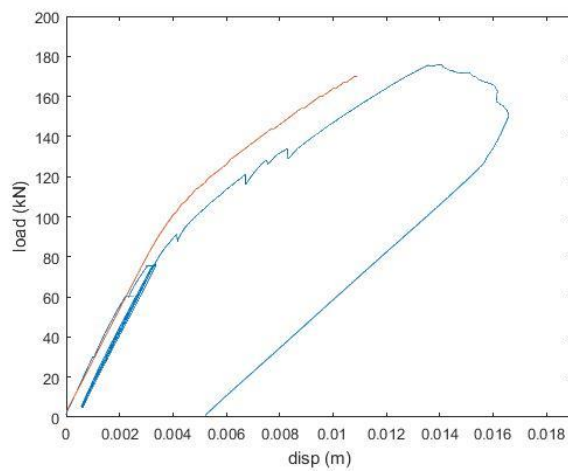


(b) mesh pattern for model V4.

Figure 3-13 Comparison of mesh pattern for model V3 and V4.

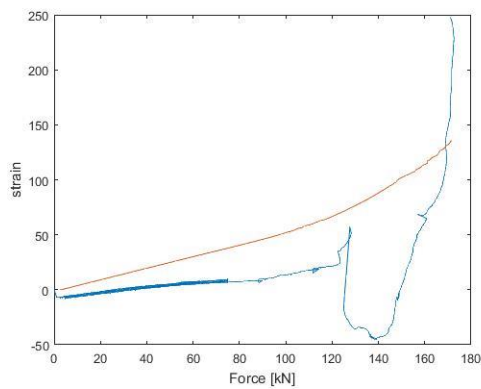


(a) breaking pattern in V4 model.

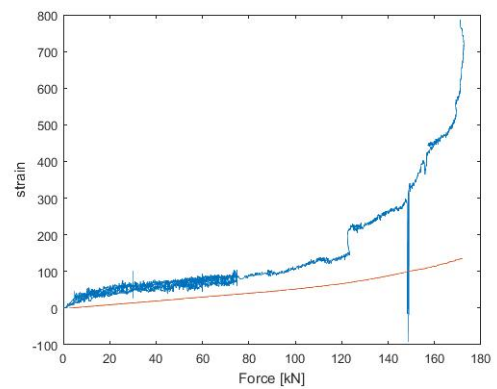


(b) Load-Displacement relationship of the model.

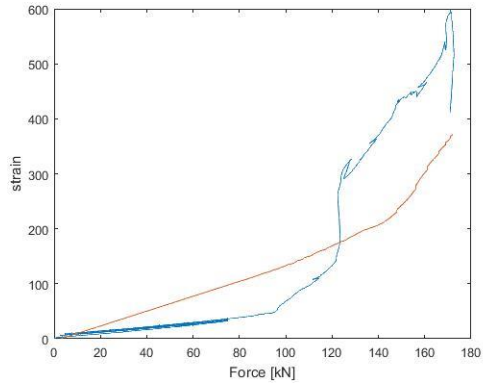
Figure 3-14 The result for V4 model.



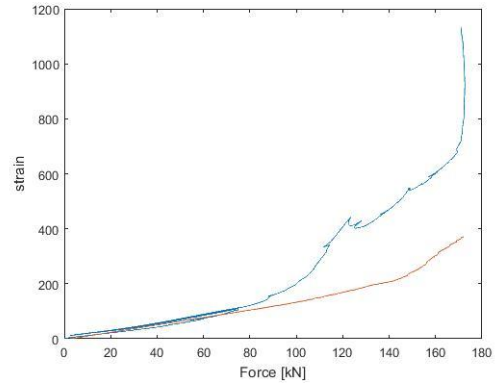
(a) monitor 1 (horizontal)



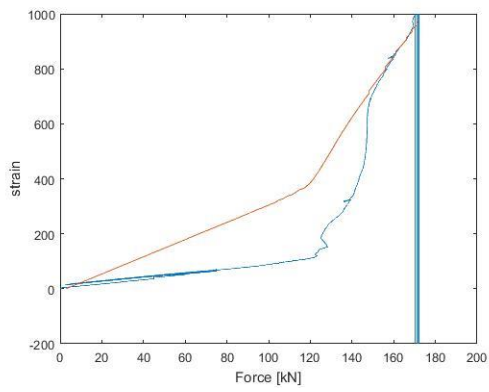
(b) monitor 2 (horizontal)



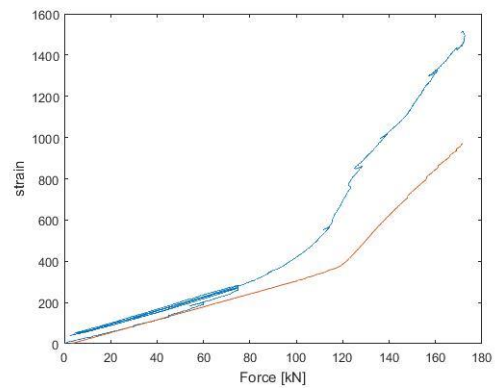
(c) monitor 4 (horizontal)



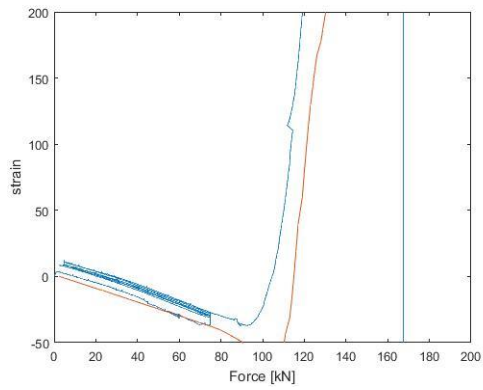
(d) monitor 5 (horizontal)



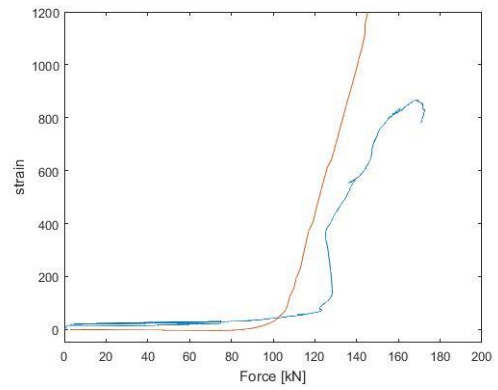
(e) monitor 6 (horizontal)



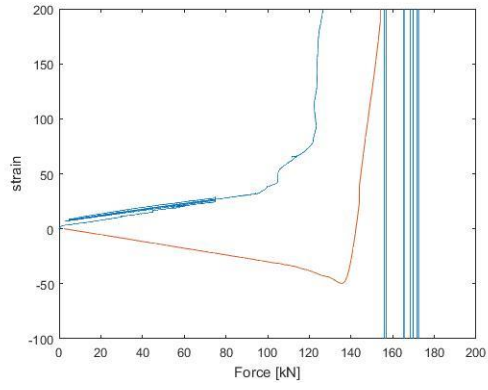
(f) monitor 7 (horizontal)



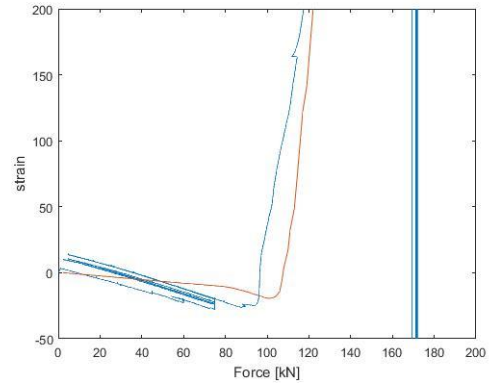
(g) monitor 8 (vertical)



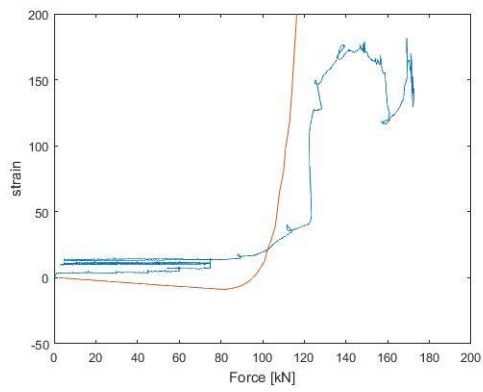
(h) monitor 9 (vertical)



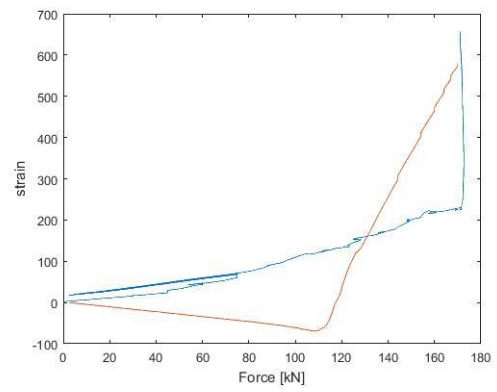
(i) monitor 10 (vertical)



(j) monitor 11 (vertical)



(k) monitor 12 (vertical)



(l) monitor 13 (vertical)

Figure 3-15 The force-strain relationship of the model.

The improvement of the **fifth model V5** is the reduction of the concrete tension strength f_t . This may not influence substantially the final result, but in ATENA Engineering if all other method have been attempted and the results still do not match the experimental evidence, it is possible to use this approach that reduce the concrete tension strength f_t to $\frac{1}{2}$ - $\frac{1}{10}$ of the original, to fine tune the results (reference [8]). This aims to represent the part of tensile capacity exhausted due to the reinforcement restraining the volume change. Figure 3-16 shows the improved result of V5. The ultimate load changes very little, compared to V4, but the curve is much closer than V4.

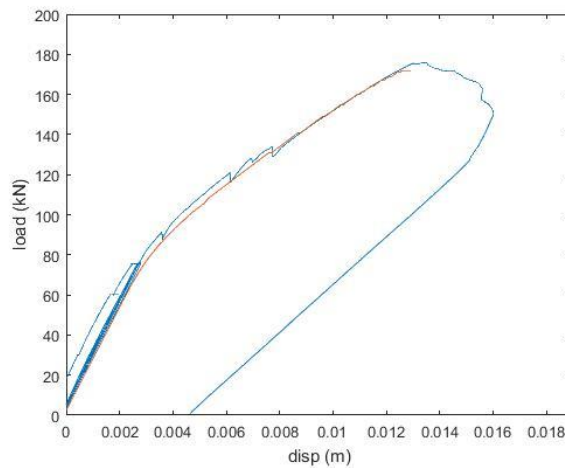


Figure 3-16 Load-Displacement relationship of V5 model.

3.2 Numerical model in ABAQUS

The previous section describes the detailed procedure to construct an accurate model in ATENA Engineering. In this section the same model will be constructed in ABAQUS, in a very similar way.

In ABAQUS users can analyze linear or non-linear models, static or dynamic problems. ABAQUS can analyze crack model by using a specific plug-in, otherwise the analysis stops at the moment when a large crack occurs, which will change the model's mechanical behavior. However, if users want to use the plug-in for the crack analysis, one small crack needs to be predefined in the pre-process, which means that ABAQUS cannot transition from an uncracked model to a crack model, but only capture the crack propagation. So it cannot describe a crack development from the very beginning. Thus, in this model the author only considered the first approach, from the unloaded (and uncracked) condition, to the formation of a crack that changes the stiffness of the model.

3.2.1 Geometry

The geometry is similar to the model in ATENA. The only difference is that in ATENA Engineering the concrete beam is divided into three parts, the slab, the web and the connection, because of the generation of brick elements, while in ABAQUS we do not need to consider this issue, because in ABAQUS one macro-element can be meshed with various types of elements and each sub-line can be treated independently, with the generation of specific seed points for the mesh. The whole model contains five parts, the concrete beam, the reinforcement and tendons, one loading plate and two support

plates. The generated mesh is shown in Figure 3-17.

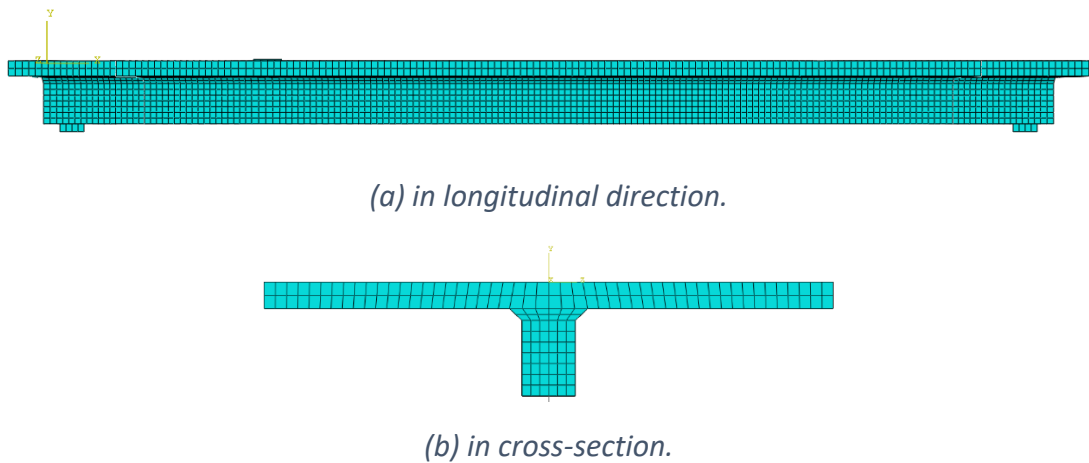


Figure 3-17 Detailed mesh generation of the model.

3.2.2 Material

The material is a little different with what is defined in ATENA. Some other parameters need to be determined in this part. The definition of the concrete model is the most significant material option that is different from the model in ATENA. In ATENA Engineering a certain concrete model is defined and after the users input the important parameters the whole stress-strain curve, the crack development and some other behaviors are generated automatically. But in ABAQUS these behaviors should be defined one by one by the users, and the users need to be familiar with the meaning of each parameter, using the Abaqus Analysis User's Guide and then input the appropriate values. With the comparison of the two different material definition, one conclusion can be obtained: in ATENA a reasonable material model can be obtained even knowing only a small number of significant parameters, while in ABAQUS a lot of other parameters, which may not be quite important, need to be determined by the users. This

means in ABAQUS the analysts have more flexibility in tuning the material model, a more accurate material behavior can be defined with more parameters measured in tests, but if the user does not have a good calibration for these not very important parameters, it is better to use the reasonable material model in ATENA, with a smaller number of significant parameters.

The material behavior of Concrete Damaged Plasticity is used in ABAQUS to define the concrete model. This model contains three parts, the plasticity, the compressive behavior and the tensile behavior. During the process, it was challenging to determine some unimportant parameters, such as the dilation angle, the eccentricity, the viscosity and so forth. For the compressive behavior, the stress and corresponding inelastic strain need to be inputted. For the tensile behavior, the GFI type is selected in this model and only the yield stress and fracture energy are needed. The following table shows the specific parameters used in the model. Moreover, the mass density, the elastic modulus and Poisson's ratio are included in the model.

Table 3-3 Concrete parameters in ABAQUS.

Density	Mass density	2300 kg/m ³
Elastic	Type	Isotropic
	Young's modulus	2.8483E+4 MPa
	Poisson's ratio	0.18
Concrete damaged plasticity	Dilation angle	33
	Eccentricity	0.1
	fb0/fc0	1.16
	K	0.667
	Viscosity parameter	0
	Compressive strength	69.7 MPa
	Tensile strength	3.343 MPa
	Fracture energy	197.05

For the steel plates the Isotropic Elastic model is used. It is similar to the material model in ATENA. Parameters are only three, mass density, elastic modulus and Poisson's ratio. These parameters are shown in Table 3-4.

Table 3-4 Steel parameters in ABAQUS (reinforcement not included).

Density	Mass density	7850 kg/m ³
Elastic	Type	Isotropic
	Young's modulus	2.8483E+4 MPa
	Poisson's ratio	0.3

The pre-stressing tendons and the reinforcement bars are in two different materials. For reinforcement, a segmented stress-strain curve is defined in ABAQUS. There is a little difference between ABAQUS and ATENA in this part. In ATENA, when defining a multi-linear material, the strain to input is the direct strain in the global coordinates, while ABAQUS needs the inelastic strain, which can be obtained with a simple

transformation. The relative parameters are presented in Table 3-5.

Table 3-5 Reinforcement parameters in ABAQUS.

Density	Mass density	7850 kg/m ³
Elastic	Type	Isotropic
	Young's modulus	1.95E+5 MPa
	Poisson's ratio	0.3
Expansion	Expansion coefficient	1.2E-5
Plastic	Yield stress / Plastic strain	560 MPa / 0
		620 MPa / 0.00682
		600 MPa / 0.01692
		400 MPa / 0.02293

The material of pre-stressing tendons is defined as an elastic-perfectly-plastic model.

The input values are shown below and the stress-strain diagram is the same represented in Figure 2-1.

Table 3-6 Pre-stressing tendon parameters in ABAQUS.

Density	Mass density	7850 kg/m ³
Elastic	Type	Isotropic
	Young's modulus	1.95E+5 MPa
	Poisson's ratio	0.3
Expansion	Expansion coefficient	1.2E-5
Plastic	Yield stress / Plastic strain	1600 MPa / 0
		1600 MPa / 0.04

3.2.3 Analysis steps and results

To have ABAQUS simulate the same loading procedure applied in the experiment, in the analysis it is best to define the loading steps in the same way. The procedure is

almost the same as what was described for ATENA Engineering, but some details are different.

The first step is the internal load. This step is modeled almost in the same way described in Section 3.1.3. The only difference is that in ABAQUS one step can be split into several small increments. The default number of increment is 100, which means that the software divides one step into 100 small steps and adds one of them in each iteration. The default amplitude function of the load increments is set to “ramp”, so each load will increase smoothly and will not create a sharp increase in loading.

The second loading is the pre-stressing load. In ATENA this pre-stressing load is divided into 10 small steps, with such load being applied to the tendons, but in ABAQUS as this direct approach does not yield good results, so a thermal expansion is used instead, to simulate the pre-stress. The temperature change calibrated and set in a way to reach the same effect. As the coefficient of thermal expansion is $1.2 \times 10^{-5} C^{-1}$, a total temperature decrease of $-330 C$ is divided into 6 loading steps, with 100 increments in each. This will provide a smooth increase of pre-stressing and result in accurate modeling.

The third load is the temperature. As mentioned before, this load captures the long-term pre-stressing loss. For this reason, the load consists only in slightly increasing the final temperature in order to decrease the pre-stressing force. So this step can be combined into the second step for the final model.

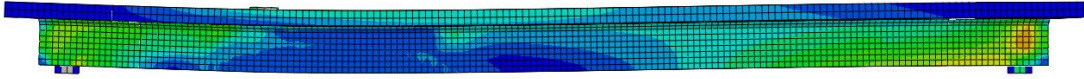
The fourth loading is the vertical load. Because this is the main load that we apply, this is the most significant part in the loading procedure. Although in ABAQUS the default

amplitude modulating function for one load is “ramp”, and each step is divided into 100 increments, additional load steps need to be introduced manually to capture the exact ultimate load. Five load steps of 20kN each are defined in the first 0 – 100 kN range, then 5 steps of 10kN each are defined in the 100 – 150 range, and then 5 kN steps are defined for the remainder of the analysis. The total loading procedure is defined in Table 3-7.

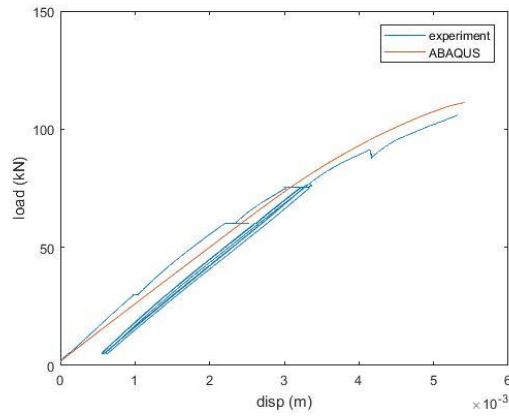
Table 3-7 Loading procedure in ABAQUS.

Load cases	Steps	Values
Temperature 0	Initial	0
Self-weight	Step 1	9.8 N/kg
Temperature 1	Step 1	-50 C° 110 MPa
Temperature 2	Step 2	-100 C° 219 MPa
Temperature 3	Step 3	-150 C° 328 MPa
Temperature 4	Step 4	-200 C° 437 MPa
Temperature 5	Step 5	-270 C° 589 MPa
Temperature 6	Step 6	-330 C° 720 MPa
Vertical load	Step 7 - 13	20 kN
Vertical load	Step 14 - 17	5 kN

The same five versions of the model, with increasing accuracy, presented in Section 3.1 have been developed also in ABAQUS, leading to the same considerations presented in the previous section. Therefore, only the results of the final model are presented here, in Figure 3-18.



(a) stress distribution after total loading procedure.



(b) load-displacement relationship of the model.

Figure 3-18 Final version of numerical model in ABAQUS.

From the figure it is clear that although ABAQUS has its limit in modeling the total crack development, it is capable of modeling where and at which point the crack happens.

Chapter 4 Mesh and Mesh Alignment in ATENA Engineering

4.1 General analysis for mesh sensitivity problem

In general, the finite element modeling in many cases is associated with the appropriate connection of structural components which are probably discretized with different network sizes and hence do not have a perfect node to node connection. Nodes and elements of one component are not congruent with the nodes and elements of the adjacent component. Engineering and scientific Finite Element software packages do have different approaches solving this problem. In particular, in this thesis the component to component connection with non-congruent element sizes and nodes are an issue of the interface between the slab and the web of the considered T-beam. Therefore, the objective of this section is to present and elaborate in more detail the procedure used for the connection of structural components in the Software package ATENA and to discuss in detail the mesh sensitivity and the influence of node positions in the contact zones on the structural response.

The discretization of a structure with a finite element mesh, no matter which element type it is, 1D truss element, 2D shell element or 3D hexahedral solid element, must ensure that each element is linked appropriate to the surrounding elements, which is also associated with a perfect node to node connection and with a correct node information.

This fundamental rule in finite element analysis guarantees the correct calculation of node results and consequently the correct determination of results in elements domains

and its boundaries by means of shape functions and post processing of stress and strain tensors in the considered and surrounding finite elements.

However, in practice, especially if the models are geometrically complex, it may happen that some issues related with the mesh go unnoticed. There are some cases that we cannot take much care of it, the carelessness of modeling, some other special reasons, these may result in a poor mesh and sometimes it may not be noticed by the users.

If users the analysts have no experimental data to be referred to as reference, or if users have few deep lack a good understanding on the whole structural behavior model, its deformed shape, its possible crack patterns and its stress distribution, they will not be able to identify the issue and determine if this model is correct. This may lead to substantial inaccuracy in the results of the analysis, which may cause serious structural problems, and potentially collapses or damages.

In ATENA Engineering one macro-element can be divided into hexahedral brick element only if this macro-element is a hexahedral body, as can be seen for the modeling of the T-beam in Chapters 2 and 3. If it is not (i.e., it has an irregular section), it will be divided into the tetrahedral element no matter which type is selected in the software. This rule ensures that the component geometry can be captured by the elements. However, in some cases the tetrahedron element cannot simulate the model perfectly and brick elements would be needed (as in the considered model). This means, the model needs to be cut into several pieces to reach the condition of brick element. However, even though you set the same element size, in different macro-elements, the mesh sizes may be different. This may confuse the users because, even when 2 macro-

elements have the same length of edge (contact with each other), as shown in Figure 4-1, this phenomena of different mesh sizes happens. In the first T-Beam models this phenomenon was not taken into account in causes errors in the structural response.

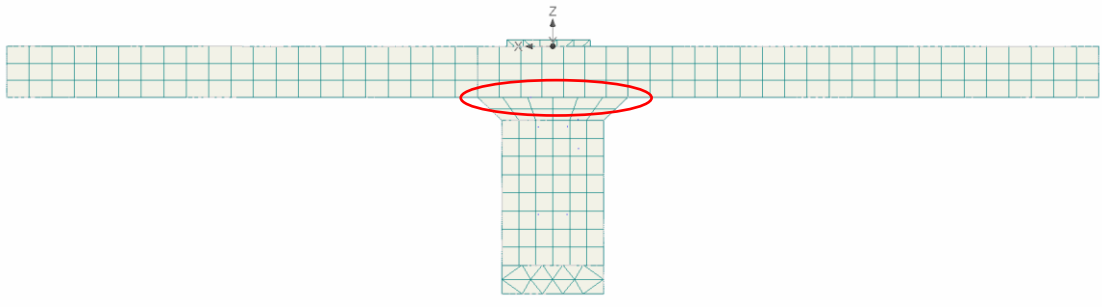
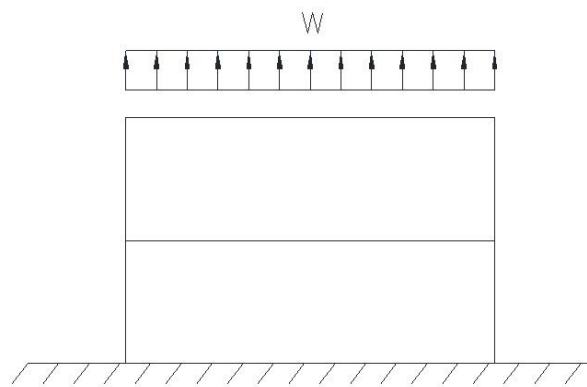


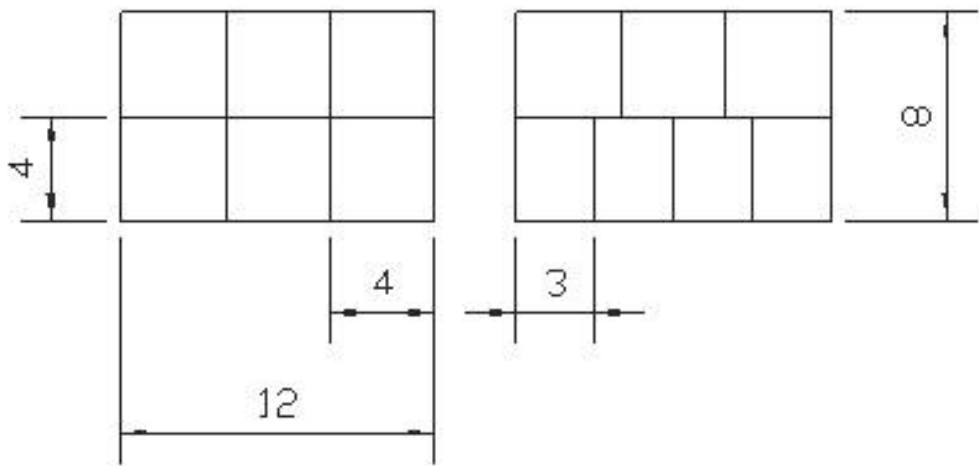
Figure 4-1 Poor mesh in the model by using automatic generation.

Besides this, a more common problem happens by connecting two macro-elements with respect to their laterally or orthogonally orientation. This contact problems between macroelements exists especially in large frame structures in which the column structures are connected to the beam structures. Column elements and beam elements are connected with constraints. In general, an atomized mesh generator is applied to such structures, which results in poor network properties in these contact areas. In addition, for complex cross-section this problem is more likely to occur. This is not due to someone's carelessness but the defect of modeling and the limitation of the software. In general, commercial software packages should address the problems outlined above by means of proper meshing and contact procedures. However, the investigations on the T-beam have shown that this is not self-evident from numerous packages. In the following, I will show what I met and interpret it with the combination of analytical theory and testing in ATENA Engineering.

Let's consider a very simple case, 4 nodes shell element with linear material and geometry named Case 1, shown in Figure 4-2 (a). An elastic plate, like steel plate is fixed along the edge, and loaded by a line distributed load at its free end. Two cases are analyzed, (a) a mesh with in line elements and nodes, and (b) a mesh with not in line elements and nodes, see Figure 4-2 (b) and Table 4-1.



(a) brief geometry and loading case for Case 1.



(b) good mesh

(c) poor mesh

Figure 4-2 Geometry and two different mesh patterns for the mesh case study 1.

Table 4-1 Mesh and material parameters in Case 1.

Material type	Elastic
Plate geometry	8×12 m
Mesh size	2 m
Ratio of mesh size between upper and lower plate in poor mesh pattern	1:0.75
Thickness t	0.1 m
Modulus of elasticity E	30×10 ⁶ Pa
Poisson's ratio ν	0.3
Distributed load w	5 kN/m

For this mesh case studies the basic equation of static analysis is

$$\{F\} = [K] \cdot \{u\} \quad (4-1)$$

where $[K]$ is the global stiffness matrix including all the information of the system.

For the determination of the stiffness matrix $[K]$ stress/strain matrix $[D]$ and the adapted matrix $[B]$ has to be calculated as follows (reference [9]):

$$[D] = \frac{E}{1-\nu^2} \cdot \begin{bmatrix} 1 & \nu & 0 \\ \nu & 1 & 0 \\ 0 & 0 & \frac{1-\nu}{2} \end{bmatrix} \quad (4-2)$$

$$[B] = \frac{1}{4ab} \cdot \begin{bmatrix} y-y_4 & 0 & y_3-y & 0 & y-y_2 & 0 & y_1-y & 0 \\ 0 & x-x_2 & 0 & x_1-x & 0 & x-x_4 & 0 & x_3-x \\ x-x_2 & y-y_4 & x_1-x & y_3-y & x-x_4 & y-y_2 & x_3-x & y_1-y \end{bmatrix} \quad (4-3)$$

Finally the stiffness matrix $[k]$ can be computed by

$$[k] = \int [B]^T [D][B] dV = \int_{x_1}^{x_2} \int_{y_1}^{y_4} t \cdot [B]^T [D][B] dydx \quad (4-4)$$

where

2a = width of each element

2b = height of each element

$[k]$ = local stiffness matrix of each element

The determination of the local stiffness matrix is based on the local coordinates of the elements, as shown in Figure 4-3.

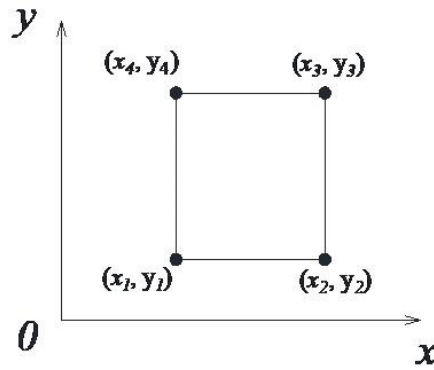


Figure 4-3 Local coordinates of each element.

The contact zone of a mesh with not in line elements and nodes are treated in ATENA Engineering with a linear combination as shown in Figure 4-4 and Table 4-2. The not inline point information is calculated from node information 1 and 2 based on the equations displayed in Table 4-2 (reference [10]).

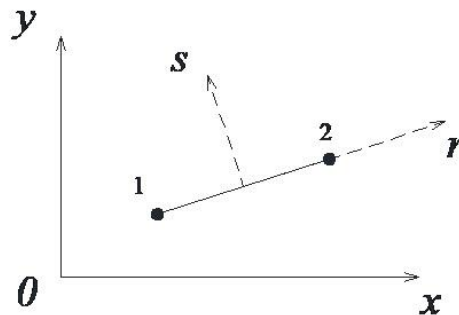


Figure 4-4 Local coordinates when dealing with the contact between macro elements.

Table 4-2 Interpolation function for the contact between nodes.

Node i	Function h_i
1	$\frac{1}{2}(1-r)$
2	$\frac{1}{2}(1+r)$

For instance, the node displacement of the not n line node can be calculated using the weighting sum approach with respect to the displacements of the adjacent two ends, using the following formulations:

$$u_i = h_1 \cdot u_1 + h_2 \cdot u_2 \quad (4-5)$$

$$v_i = h_1 \cdot v_1 + h_2 \cdot v_2 \quad (4-6)$$

These equations finally are included in the global matrices formulations and are in consequence participating in the computation of the displacements of the nodes of the whole domain due to the defined load cases.

In the following case study a line distributed load has been used.

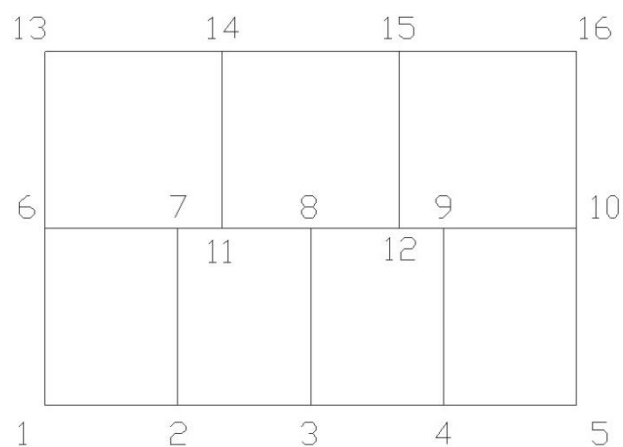


Figure 4-5 Poor mesh with all nodes numbered.

Figure 4-5 presents the mesh layout and its numbered nodes. For poor mesh we number all the nodes, as shown in figure, but we neglect node 11 and 12 and only use the rest nodes in the final displacement matrix. So we need a transform matrix $[T]$ to link the two displacement matrices. For the determination of master or slave surface, as in this problem both of them have the same section and from the load case we cannot decide which one is the main deformed body without additional constraints, so it's not necessary for each one whether it is master surface or not. Here we choose the lower plate with smaller mesh size as the master surface, and the other is the slave one. From the additional constraints node 11 and 12 can be represented using equations 4-5 and 4-6, then the transform matrix $[T]$ is generated below.

$$\{u\} = \begin{Bmatrix} u_1 \\ M \\ u_{11} \\ u_{12} \\ M \\ u_{16} \end{Bmatrix} = \begin{bmatrix} 1 & 0 & L & 0 & 0 & 0 & 0 & 0 & L & 0 \\ M & & & & & & & & & M \\ 0 & 0 & L & 0.665 & 0.335 & 0 & 0 & 0 & L & 0 \\ 0 & 0 & & 0 & 0.335 & 0.665 & 0 & 0 & L & 0 \\ M & & & & & & & & & M \\ 0 & 0 & L & 0 & 0 & 0 & 0 & 0 & L & 1 \end{bmatrix} \begin{Bmatrix} u_1 \\ u_2 \\ M \\ u_7 \\ u_8 \\ u_9 \\ u_{10} \\ u_{13} \\ M \\ u_{16} \end{Bmatrix} \quad (4-7)$$

$$\{u\} = [T]\{\hat{u}\} \quad (4-8)$$

Replacing Equation 4-8 into 4-1 and pre-multiplying by $[T]^T$ yields the modified system

$$\{\hat{F}\} = [\hat{K}]\{\hat{u}\} \quad (4-9)$$

in which

$$[\hat{K}] = [T]^T [K] [T] \quad (4-10)$$

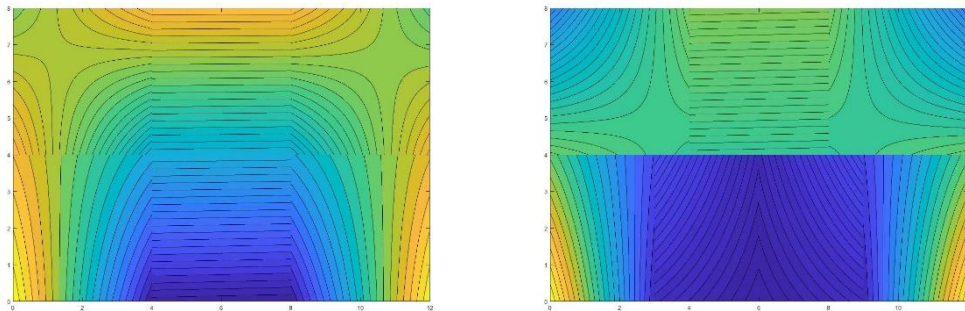
$$\{\hat{F}\} = [T]^T \{F\} \quad (4-11)$$

Equation 4-9 is a new linear system containing 14 equations in the remaining 14 unknowns:

From this equation we could get the displacement of each node in two directions. In this algorithm we can substitute these calculated nodal displacement into local coordinates and then get the stress of each point in one element.

Good mesh and poor mesh

From this equation we can get a stress distribution diagram shown below. The x and y axis represent the geometry of the plate.

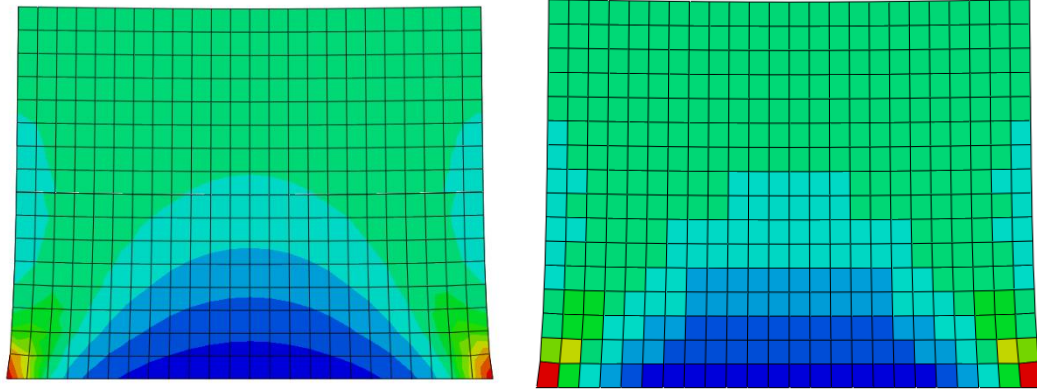


(a) good mesh

(b) poor mesh

Figure 4-6 Stress distributions calculated by using algorithm above.

Let's compare it with the same model in ABAQUS. I construct the same model in ABAQUS inputting those parameters shown above. The stress distribution in ABAQUS shown in Figure 4-7.



(a) with averaging the stress

(b) without averaging

Figure 4-7 Stress distributions for Case 1 in ABAQUS with finer mesh.

By default, only four points near the corners in the shell element are considered in the calculation. Then, an average calculation is used to measure the other points with respect to the distance between points. So it may vary with the result, which varies smoothly.

In this approach the stress distribution generated in ABAQUS is shown in Figure 4-7 (a). However, we mute this option and draw the same diagram, only the stress in the middle represents the whole element and the plot is Figure 4-7 (b). With the comparison we could easily see that the left figure is much finer and smoother than the right. In the left figure each element is divided into several colors representing different stress while in the right one each element is only painted in one color. Comparing these figures with what is obtained in MATLAB, we could know that in perfect linear condition these two results are close to each other in good mesh.

Now we turn to the worse net. Tables show the two results. Comparing the results

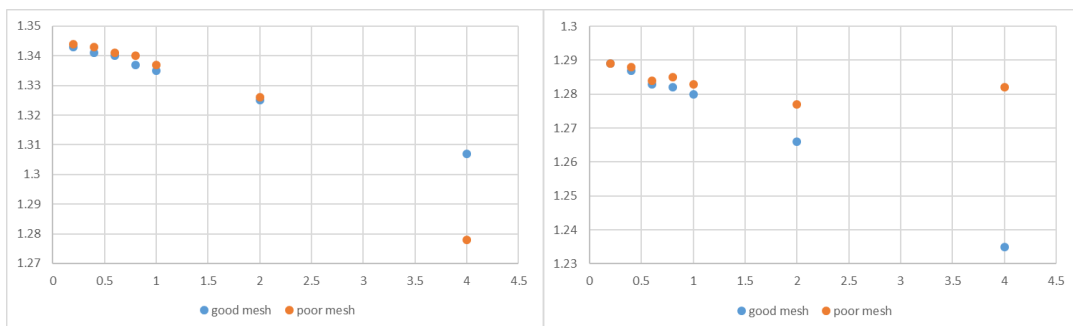
between the good mesh and the poorer mesh, we found that these two results are close to each other for the displacement of the contact when the element size is small enough.

Table 4-3 Displacement of different mesh patterns at point 16.

Displacement of different mesh patterns (corner point, scale E-2)				
element size	fine mesh	coarse mesh	deviation	element number
4	1.307	1.278	-0.029	7
2	1.325	1.326	0.001	36
1	1.335	1.337	0.002	128
0.8	1.337	1.34	0.003	215
0.6	1.34	1.341	0.001	374
0.4	1.341	1.343	0.002	820
0.2	1.343	1.344	0.001	3280

Table 4-4 Displacement of different mesh patterns at point 15.

Displacement of different mesh patterns (inner point, scale E-2)				
element size	fine mesh	coarse mesh	deviation	element number
4	1.235	1.282	0.047	7
2	1.266	1.277	0.011	36
1	1.28	1.283	0.003	128
0.8	1.282	1.285	0.003	215
0.6	1.283	1.284	0.001	374
0.4	1.287	1.288	0.001	820
0.2	1.289	1.289	0	3280



(a) stress at point 16

(b) stress at point 15

Figure 4-8 Difference between good mesh and poor mesh.

Now we change another problem to see how it works near the contact, not far away from it (like node 16). In this new problem (named Case 2) smaller mesh is generated both in good mesh and poor mesh patterns. The mesh size is certain, one is 4×6 with all nodes on lines while the other is not. Detailed geometry is shown in Figure 4-5. As the MATLAB codes are a simplified algorithm based on the ATENA calculation, we now construct the same model in ATENA Engineering and see its performance. The following charts are the results in ATENA and ABAQUS. The methodology in ATENA Engineering is totally different with ABAQUS. For ATENA it calculates the displacement and strain of each point in one element but for ABAQUS it calculates displacement and strain of 4 points in one element and then uses average method to obtain the other points.

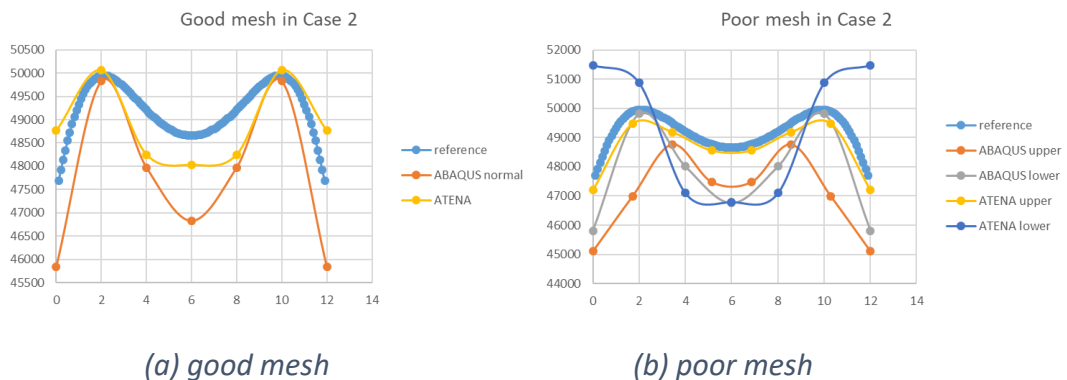


Figure 4-9 The stresses along the contact.

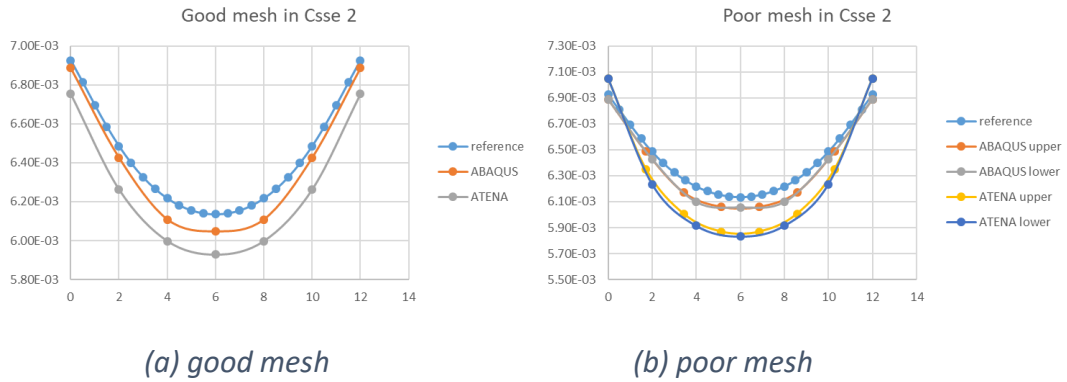


Figure 4-10 The displacements along the contact.

The analysis above focuses only on one-dimensional poor mesh, however, you have to be aware in most cases two-dimensional poor mesh occurs on the contacts, see Figure 4-11. In two-dimensional meshes, the outer node is not in the line at one edge, but within the element and lies on the surface. The detailed picture is shown below.

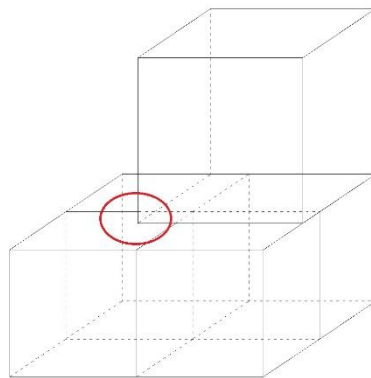


Figure 4-11 General appearance of 2 dimensional poor mesh.

This two-dimensional poor mesh is more likely to happen in practice if users do not care about it. Now we use a simply supported concrete beam to see its accuracy in a simple load case. This is the new case (named Case 4) that the mesh of connection is

not compatible with the slab and the web. The nodes are not laid perfectly on the mesh line. The geometry of the concrete beam is shown below, with two steel bars in the longitudinal direction. The detailed parameters of concrete and reinforcement are shown in Figure 3-4 and 3-6. These materials are the same as using in the T-shape beam. The crack pattern is shown below together with a table including the displacement below loading plate and the ultimate load of this structure.

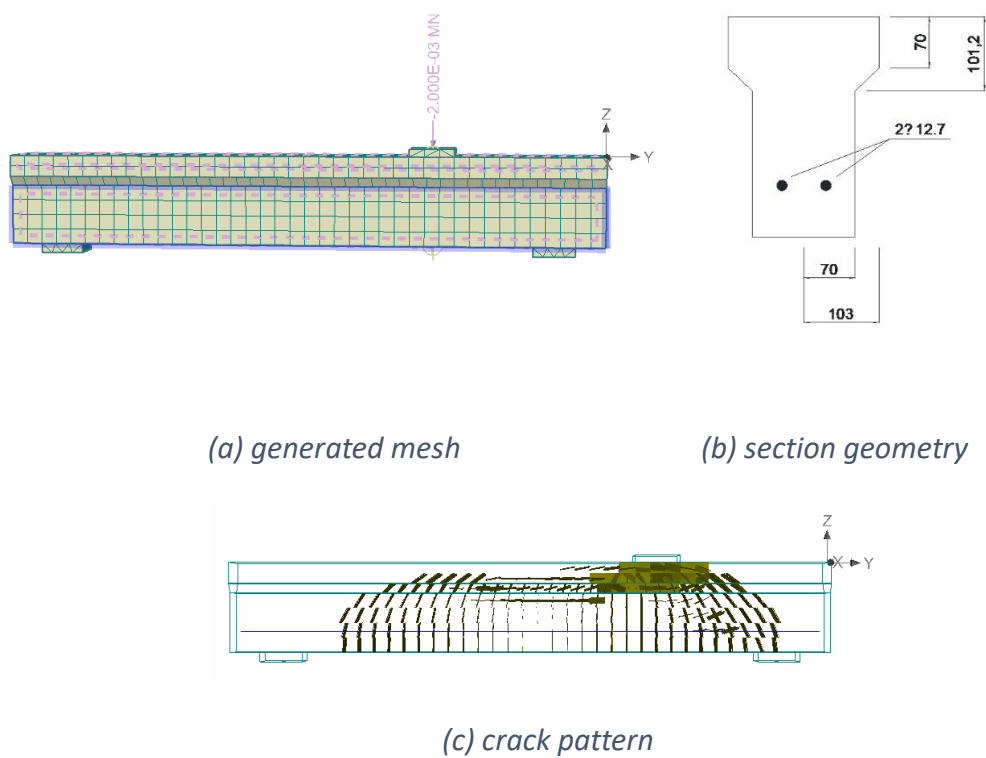


Figure 4-12 Detailed information about Case 4.

Table 4-5 Comparison of 3 test cases.

Mesh case	Crack load (kN)	Ultimate load (kN)	Ultimate displacement (mm)
good mesh	16	132	5.04
1D poor mesh	16	132	5.04
2D poor mesh	16	128	4.60

From the table it is clearly seen that for one-dimensional poor mesh the result is close to the good mesh, but if it comes to two dimensional poor mesh, the result differs a lot. It decreases nearly 8.7% of origin for the displacement and if the stress near the contact is considered the difference of results is much larger.

4.2 Nodal distance

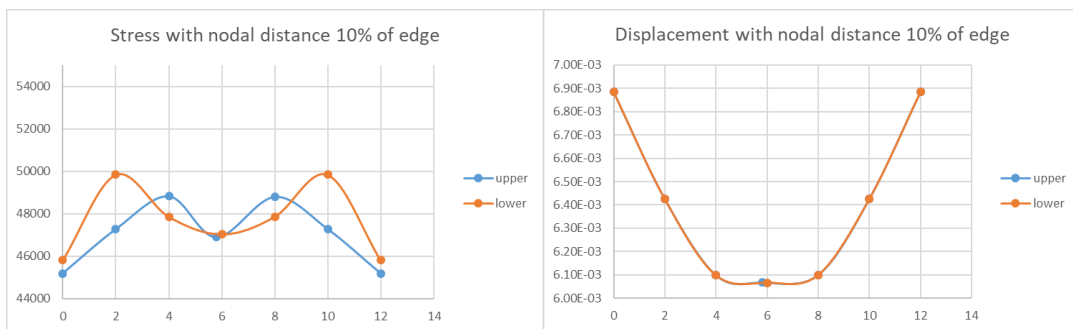
In this section, the focus is still on mesh sensitivity, analyzing in particular the location and deformation of the nodes the “nodal distance”.

Nodal distance means the distance between two nodes which should be linked perfectly in a good mesh. As discussed before, in practice users may result in the mesh sensitivity problems even though they do not notice it. For a very simple problem, one beam and one column are constructed and meshed separately and then assembled together, node problem may occurred in the contact surface. In many commercial engineering software this kind of constraint, automatically added or needed to be defined by the users, exists in order to deal with this type of problems. As this algorithm is coded in these software, the accuracy of their results should be totally considered in case someone does this operation and get one certain result, but this result is far away from the most accurate one. How this distance influences the results? In which cases can we ignore its effect? The objective of this chapter is the analyses and discussion of the “nodal distance” approach.

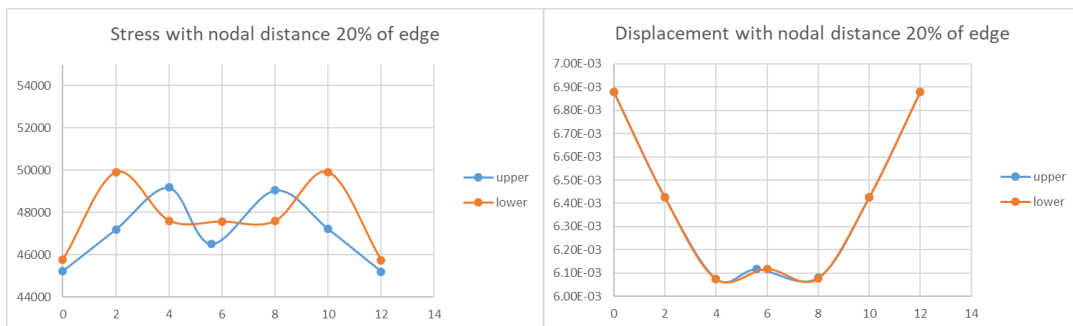
A new case is designed for this problem. It's similar to the problem above but the position of middle nodes in the upper plate is varying with the increasing nodal distance Δ .

The element size is 2 m and the increment of nodal distance is 0.2 m (10 percent) in each model. The stress and displacement is presented below along its location. Because of the same reason attached above, the stress is calculated and distributed in each macro-element, so for those points related to two element (or four element), especially

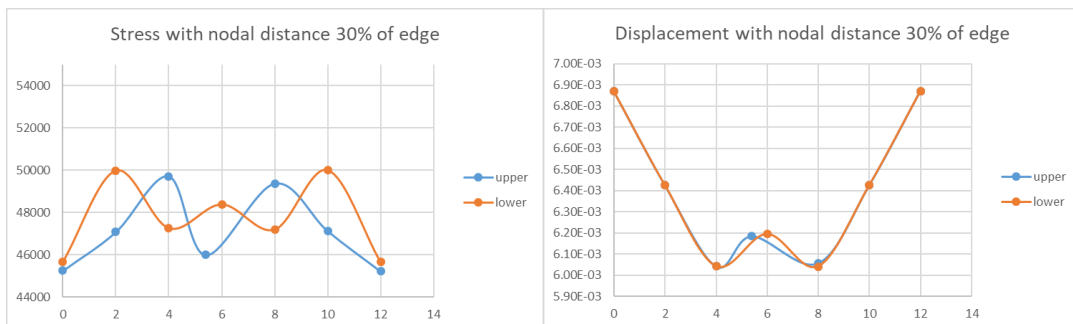
on the contact, suffer two values of stress, belonging to upper plate and lower plate. In this case two distributed curves are generated, upper and lower stress, to see the influence of the changes of nodal distance. The detailed figures are shown below. The units in the graphs are for the vertical axes Pascal (stress) and the horizontal axes meter (displacements) along the contact.



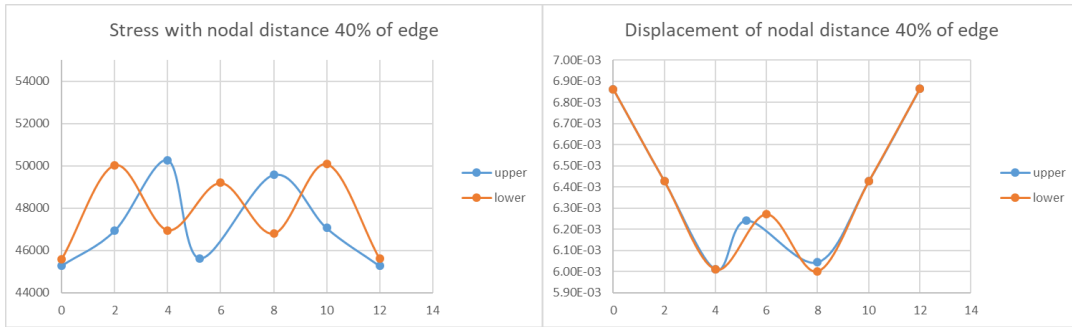
(a) stress and displacement along the contact with nodal distance 10% of edge.



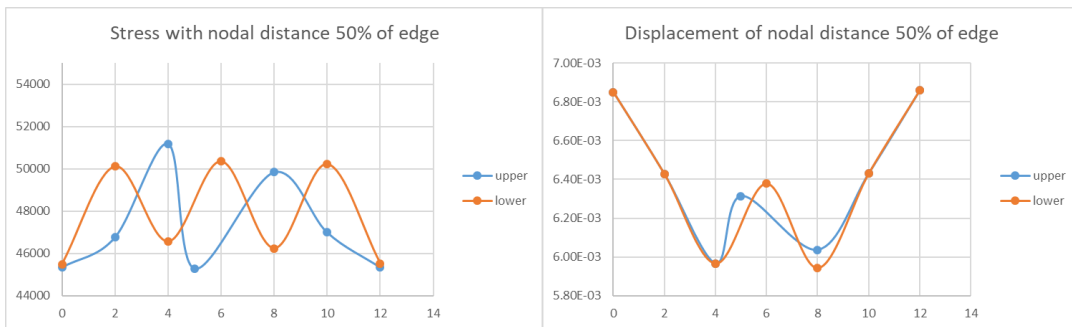
(b) stress and displacement along the contact with nodal distance 20% of edge.



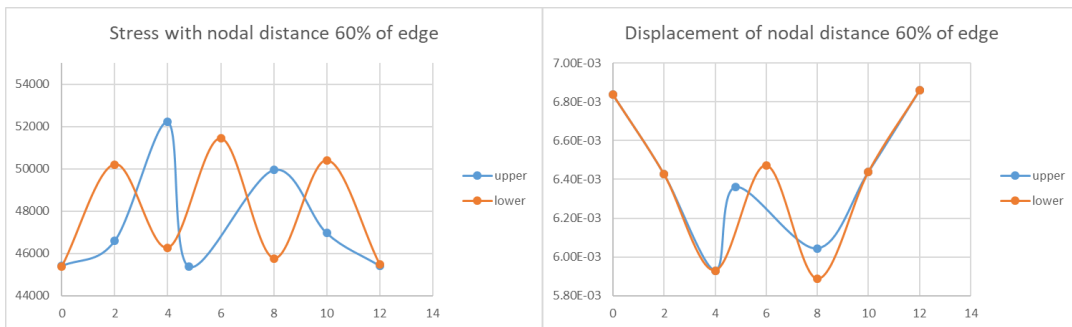
(c) stress and displacement along the contact with nodal distance 30% of edge.



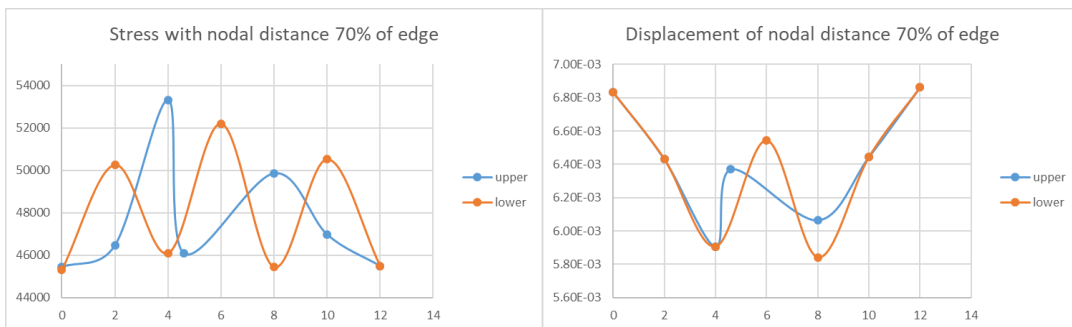
(d) stress and displacement along the contact with nodal distance 40% of edge.



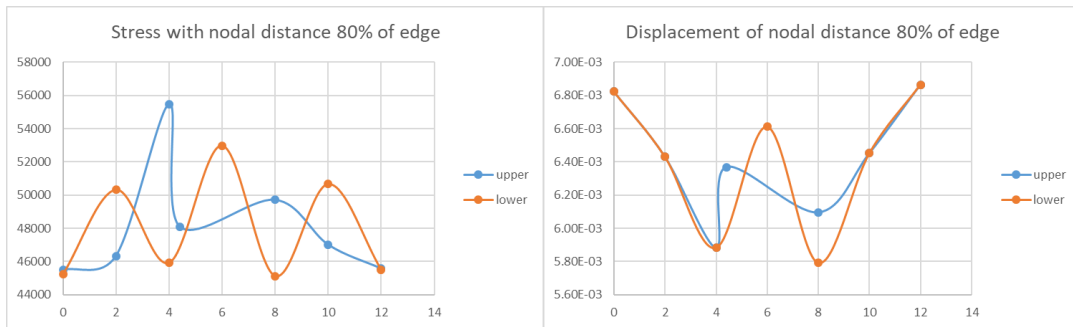
(e) stress and displacement along the contact with nodal distance 50% of edge.



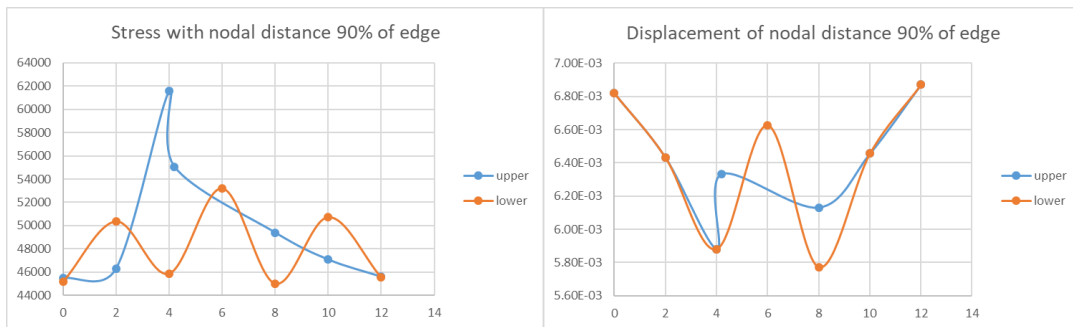
(f) stress and displacement along the contact with nodal distance 60% of edge.



(g) stress and displacement along the contact with nodal distance 70% of edge.



(h) stress and displacement along the contact with nodal distance 80% of edge.



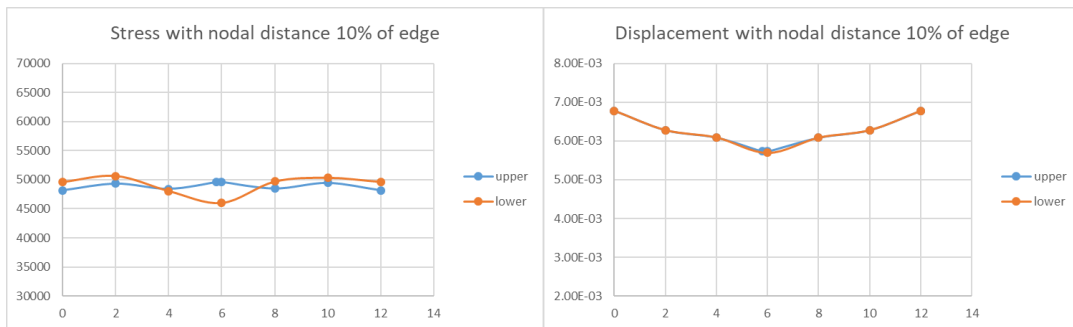
(i) stress and displacement along the contact with nodal distance 90% of edge.

Figure 4-13 Stress and displacement developments along the contact with nodal distance increasing in ABAQUS.

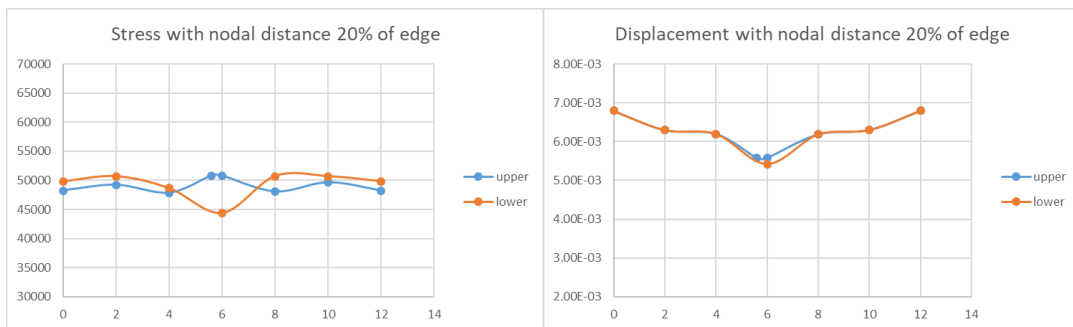
From these figures it is clearly seen that the nodal distance is larger, the stress and displacement is less accurate. With Δ only 10 or 20 percent of mesh size, the figures are similar to each other and they are all close to the exact result shown in Figure 4-9 above. However, when it goes to 40 percent, in the stress chart (the left column) the middle point of lower plate becomes larger and far away from the exact value. It becomes a peak value compared with the adjacent points monitored nearby while it should be flat and a little lower than the other two. For the displacement it has been already shown in Figure 4-10 that the largest displacement occurs at its two edge and the smallest displacement is in the middle. While in the displacement chart (the right column) the

middle displacement increases in the same pace of nodal distance varying. In the first two graphs (10 to 20 percent) the displacement in the middle does not differ a lot from the exact value. When the nodal distance is up to 40 percent, the displacement in the middle becomes a large value, instead of the adjacent points it is closer to the second near points.

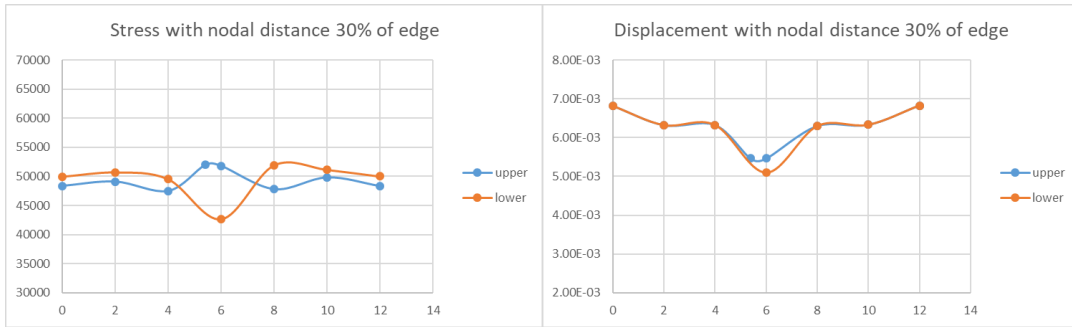
In ATENA Engineering the development in these two aspects is similar to what is shown in ABAQUS. The curve along the contact may be a little different but the development with Δ increasing is the same. The developed figures are shown below.



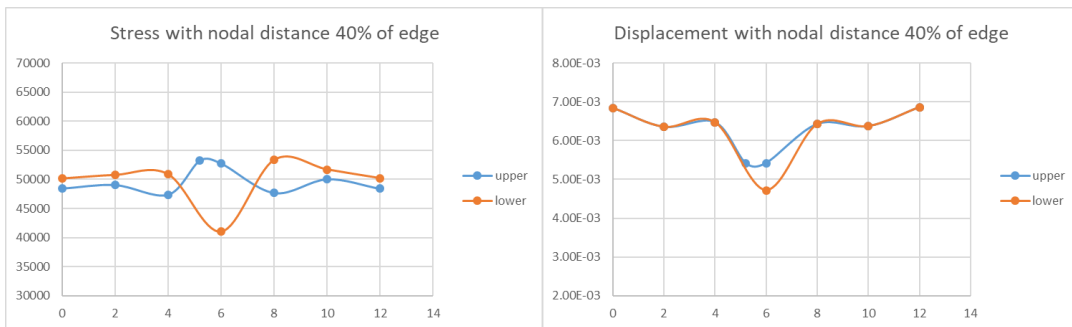
(a) stress and displacement along the contact with nodal distance 10% of edge.



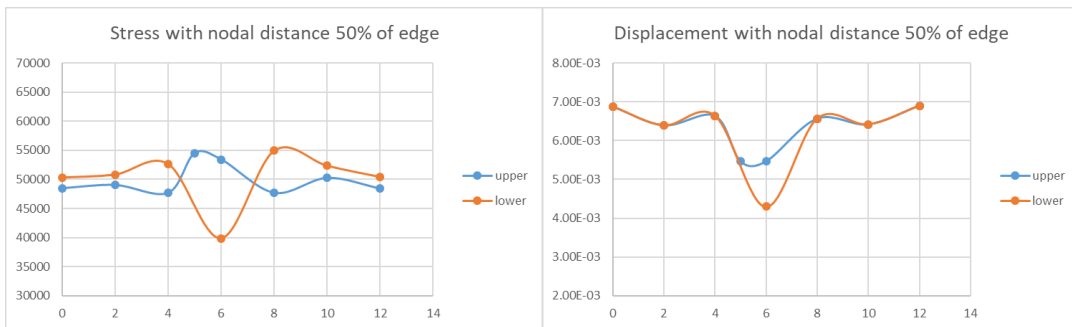
(b) stress and displacement along the contact with nodal distance 20% of edge.



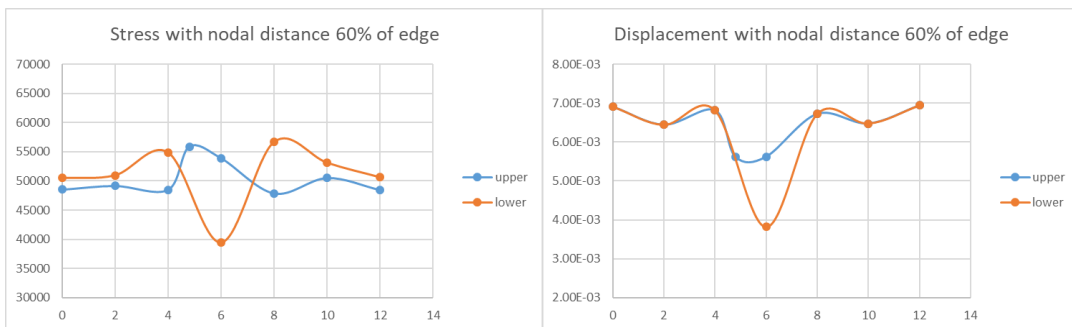
(c) stress and displacement along the contact with nodal distance 30% of edge.



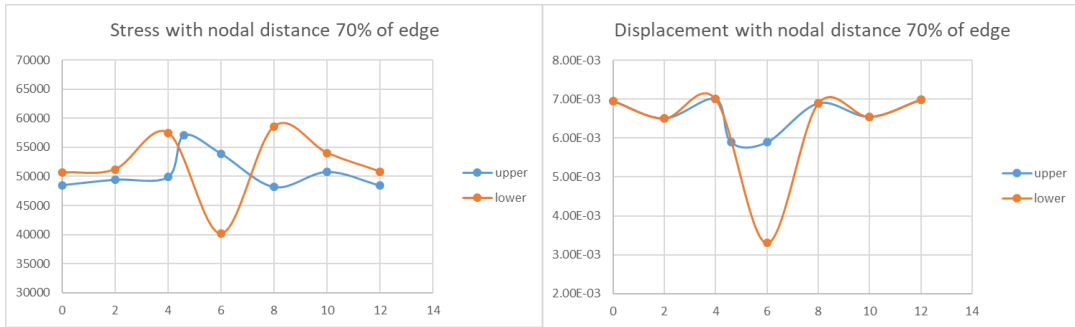
(d) stress and displacement along the contact with nodal distance 40% of edge.



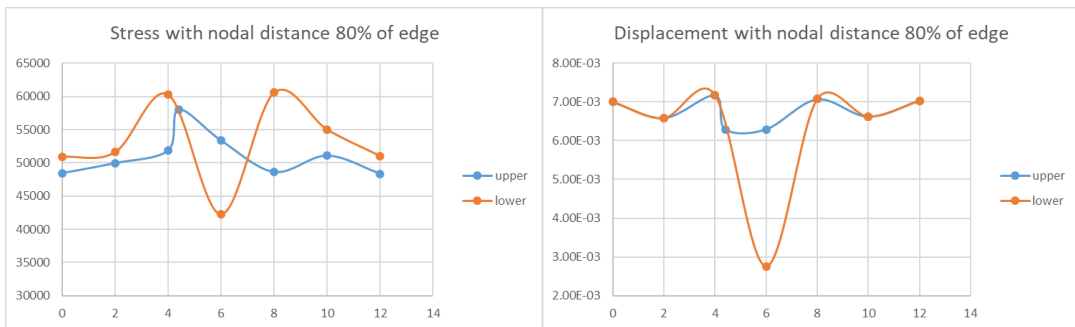
(e) stress and displacement along the contact with nodal distance 50% of edge.



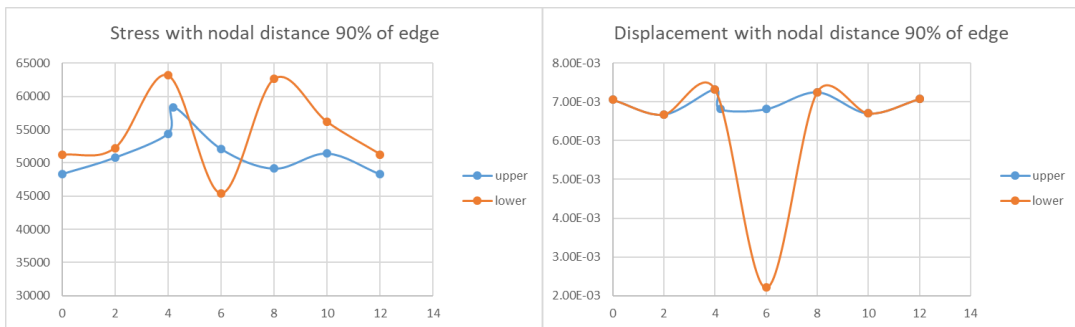
(f) stress and displacement along the contact with nodal distance 60% of edge.



(g) stress and displacement along the contact with nodal distance 70% of edge.



(h) stress and displacement along the contact with nodal distance 80% of edge.



(i) stress and displacement along the contact with nodal distance 90% of edge.

Figure 4-14 The stress and displacement developments along the contact with nodal distance increasing in ATENA Engineering.

With the same influence in ABAQUS, in ATENA 30 to 40 percent is a limit to the results. If nodal distance Δ is larger than 40 percent of edge (0.8 m), the final results differ a lot to the theoretical value and the distributions of them along the contact become irregular and distorted.

From the analysis above no matter what aspect is concerned, the stress or displacement, the middle point in the lower plate varies largest with nodal distance Δ increasing. Now the value of this point is only considered along the nodal distance Δ varying in order to see the development of the stress and displacement.

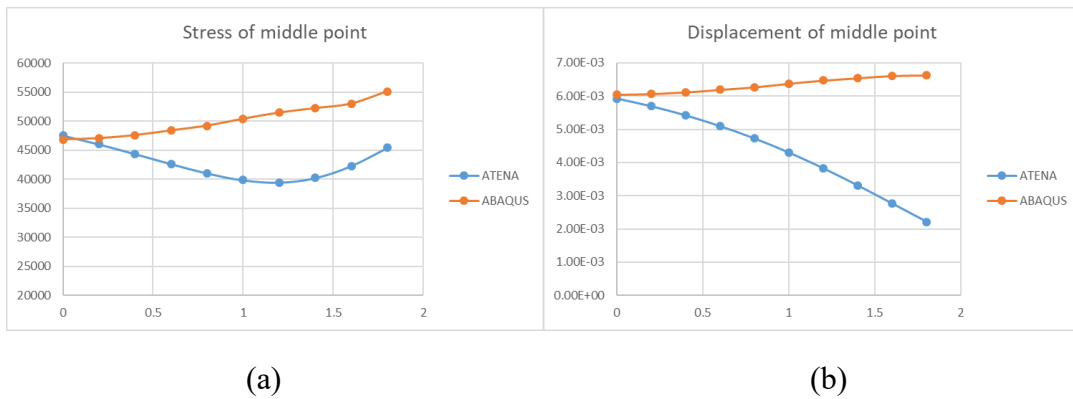


Figure 4-15 Development of stress and displacement at middle point along with nodal displacement Δ increasing.

All of these data are calculated and selected in the lower plate. The x axis represents nodal distance Δ (m), and y axis are Pascal and meter separately. From these figures it is seen that both in ATENA and ABAQUS the stress and displacement vary along with nodal distance Δ increasing, but there are some differences between them. For stress development, the middle stress in ABAQUS increases all the way while in ATENA it gets down first and after 1.2 m it rise up and finally it returns to about 45000 Pa. But this is not the recovery. In Figure 4-15 above the larger Δ affects a much more twisted distribution both in stress and displacement if Δ is larger than 1.2 m (60 percent). So the more nodal distance Δ is set, the more inaccuracy the results get for the stress of

middle point. For displacement development, the result is the same. The only difference between ATENA and ABAQUS is that with Δ increasing the middle displacement decreases in ATENA while it rises in ABAQUS, and the amplitude between two software is different, ATENA is larger than ABAQUS.

Chapter 5 Differences in commercial software products

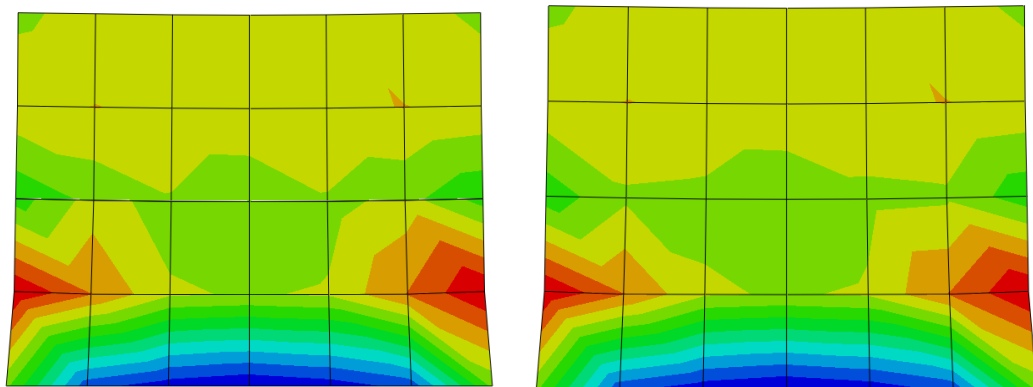
In a further investigation, the goal was to compare and analyze the results of the software ATENA and ABAQUS. Both of these commercial software products are widely used and known in Europe and worldwide.

These two software products differ significantly in the discretization routine (mesh generator), the implemented material laws, the solving algorithms, the user interface, the visualization among others. The essential differences for the above described analyzes in the sections above are outlined below;

1. Theoretical consideration. In ATENA Engineering and ATENA Science, the analysis is performed on the basis of the Lagrangian formulations and configuration at the time of the respective iteration. ATENA Engineering also allows the determination of the strain and displacement of each element in the element algorithm to be calculated directly. This means that the elements in the element calculation part are off when a contact is added, meaning that a part divided into two parts is not the same as before, and in that case the result has to be changed. For these specific cases, the results of these two cases are with or without contact.

While in ABAQUS things get different. Instead of all of the stress and displacement in one element calculated by the same algorithm, only on nodes are calculated, which means the users can only get those values at ends in truss or corners in shell and hexahedral element. The other values inside the element is calculated by linear averaging in one macro-element. Here is the difference. One simple case is considered

here in ABAQUS, the same geometry, load pattern, boundary condition and mesh pattern with one having a contact in its middle and one without. The results show clearly in Figure 5-1 that the one without contact have a much smooth change in stress while the other is cut off at the contact. And comparing the values at nodes, these two results do not have large difference (shown in Figure 5-1 and 5-2).



(a) with contact in the middle

(b) without contact in the middle

Figure 5-1 Comparison of stress distributions with and without contact.

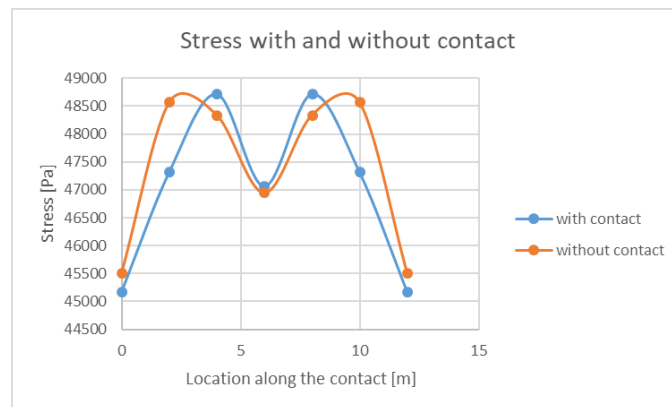


Figure 5-2 Comparison of stress with and without the contact.

2. Visualization. ATENA presents the load and deformations in the nodes in number

format, it allows the user only indirectly access to the stress distributions. The presentation of the deformed structure as well as the crack pattern is very user-friendly in ATENA. The crack properties such as width, orientation, inclination are automatically displayed in the integration points of the elements by ATENA. In ABAQUS this form of presentation is only limited. The characterization of the crack properties in ABAQUS can be derived from the stress distribution and the deformations in the nodes.

3. Computation cost: The computational effort in ABAQUS is much smaller than that in ATENA Engineering. The loading procedure in ATENA significantly differs from that of ABAQUS ATENA requires the definition of small loading increments, while many iterations are used in the increment for balancing internal and external energy while in ABAQUS a large step can be defined and it runs in ramp function with lots of increments. For the analyses T-Beam (see sections above) ATENA requires more than 160 steps while ABAQUS requires only 15 steps. All of these result in a large difference in calculation. For my model in ABAQUS it spends less than 1 hour while in ATENA Engineering it needs more than 6 hours.

4. Main focuses of the software products. ABAQUS contains almost all the models and users can do everything they want in this software, not focusing on one certain aspect, but can do steel analysis or concrete analysis (allocated in materials), building analysis, tower analysis or dam analysis (allocated in structure types). However, this results in a lot of different types of models existing in ABAQUS (both in material and element) and users need to get a full understanding of this software before constructing a model, a

wide cover means much more parameters need to be set precisely. Otherwise the result will be far away from the real. In a word, ABAQUS needs a lot of learning and a total understanding before using it.

ATENA Engineering is a software focusing only on the concrete analysis (of course steel analysis can be done in ATENA but this is not the main aspect). It is much convenient in concrete study than ABAQUS, especially in the material part. In ATENA it inserts a reasonable concrete model and when users input the cube compressive strength it will generate many default values automatically. Besides this, in ATENA only some significant parameters need to be input and in many cases users can just remain these default values. This means the spent of time in learning and understanding of ATENA Engineering is much shorting than that in ABAQUS.

5. ATENA Engineering can analyze the total crack development, from the very beginning to the break moment, while ABAQUS can analyze either the uncracked part or the cracking process, which cannot be combined into one model. ATENA Engineering overestimate the crack a little, which means at some area the crack occurs in the simulation while it won't in the real test. On the opposite, ABAQUS underestimated the crack a little, it will not show some cracks on its stress figure although it will happen in practice.

Chapter 6 Conclusion

The combined shear and flexure performance of pre-stressing concrete T-shape beam is analyzed in both ATENA Engineering and ABAQUS. In particular, the thesis analyzes the influence of mesh sensitivity and nodal distance in the contact areas, to see how different meshes in the contact areas can affect the results. Some conclusions can be drawn.

1. ATENA Engineering is effective in calculating the results even with a poor mesh.

The contact model that uses a linear combination of the nodal displacements does well in estimating the displacement field, but has some problems when calculating the stress distribution near the contacts.

2. The approach is particularly effective with one-dimensional models, where even a poor mesh is compensated by the contact model if the mesh size is small enough, but when it comes to a two-dimensional poor mesh, the linear combination will not yield good results.

3. The contact model (offered as default modeling step in these software packages) works well in most cases, but if the analyst happens encounter one of the special cases where the contact model does not work, without noticing it, the result can be very inaccurate, and this can lead to serious problems.

4. ATENA Engineering spends much more time in analyzing a certain model than ABAQUS, while ABAQUS is more difficult for users if they do not user it before in

concrete analysis. ATENA Engineering has defined a lot of reasonable material models which can help users be familiar with this software fast.

References

- [1] Tong T., Liu Z., Zhang J., Yu Q. (2016). Long-term performance of prestressed concrete bridges under the intertwined effects of concrete damage, static creep and traffic-induced cyclic creep. *Engineering Structures* 127, 510-524.
- [2] Strauss, A., Krug, B., Slowik, O., Novak, D. (2017). Combined shear and flexure performance of prestressing concrete T-shaped beams: Experiment and deterministic modeling. *Structural Concrete, FIB*, 1-20.
- [3] Sajdlova, T. (2016). Tutorial for ATENA Science GiD FRC. Prague: Cervenka Consulting Ltd.
- [4] Peirce, Daniel, Robert J. Asaro, and A. Needleman (1988). Material rate dependence and localized deformation in crystalline solids. *Computer Methods in Applied Mechanics and Engineering*, 69-85.
- [5] Munjiza, A., and N. W. M. John (2002). Mesh size sensitivity of the combined FEM/DEM fracture and fragmentation algorithms. *Engineering Fracture Mechanics* 69, 281-295.
- [6] CEN (2004). Eurocode 2: Design of Concrete Structures—Part 1-1: General Rules and Rules for Buildings. Vol. BS EN 1992-1-1:2004. Science and Education Publishing.
- [7] Strauss, A., Castillo, P., Bergmeister, K., Krug, B., Wendner, R. W., Matos, J., Casas, J. R. (2018). Shear performance mechanism description using digital image correlation. *Structural Engineering International*, 338-346.
- [8] Pryl D, Cervenka J (2013). ATENA Troubleshooting. Prague: Cervenka Consulting

Ltd.

[9] Logan, Daryl L (2011). A first course in the finite element method. Cengage Learning.

[10] Červenka, Vladimír, and Libor Jendele (2007). ATENA Theory. Praha, Czech Republic.

[11] Hibbit, Karlsson, and S. Inc. ABAQUS User Guide V. 6.6. Pawtucket: HKS Inc.

Chapter 7 Brief biography



Xingjian Wang

Shenyang, China. 11/10/1994.

Parents: Hanjun Wang and Run Zhang

Master student in Department of Civil and Environmental
Engineering